Schistosoma mansoni antigen induced innate immune memory features mitochondrial biogenesis and can be inhibited by ovarian produced hormones

Juan Marcos Oviedo[1], Diana Cortes-Selva[1], Marco Marchetti[2], Lauren Gordon[3], Lisa Gibbs[1], J. Alan Maschek [6,7], James Cox[4,6], Seth Frietze[5], Eyal Amiel[5], Keke C. Fairfax [1,8]

[1] Department of Pathology, Division of Microbiology and Immunology, University of Utah, Salt Lake City UT, 84112
[2]Department of Human Genetics, Utah Center for Genetic Discovery, University of Utah, Salt Lake City, UT, 84112, USA
[3]Meharry Medical College, Nashville TN, 37208
[4] Department of Biochemistry, University of Utah, Salt Lake City UT, 84112
[5] Department of Biomedical and Health Sciences, University of Vermont, Burlington, VT 05405
[6]Metabolomics, Proteomics and Mass Spectrometry Cores, University of Utah, Salt Lake City, UT, 84112
[7] Department of Nutrition and Integrative Physiology and the Diabetes and Metabolism Research Center, University of Utah, Salt Lake City, UT 84112

[8]Corresponding author

Keke Fairfax
Department of Pathology
Division of Microbiology and Immunology
University of Utah
JMRB 2200B
15 N Medical Drive East
Salt Lake City, UT 84112
Email: keke.fairfax@path.utah.edu
ORCID: https://orcid.org/0000-0002-8382-2960
801-581-5980 (office)

Abstract

We have previously identified that *S. mansoni* infection induces a unique form of myeloid training that protects male but not female mice from high fat diet induced disease. Here we demonstrate that ovarian derived hormones account for this sex specific difference. Ovariectomy of females prior to infection permits metabolic reprogramming of the myeloid lineage, with

BMDM exhibiting carbon source flexibility for cellular respiration, and mice protected from systemic metabolic disease. The innate training phenotype of infection can be replicated by *in vivo* injection of SEA, and by exposure of bone marrow to SEA in culture prior to macrophage differentiation (Day 0). This protective phenotype is linked to increased chromatin accessibility of lipid and mitochondrial pathways in BMDM including Nrf1 and Tfam, as well as mitochondrial biogenesis. This work provides evidence that *S. mansoni* antigens induce a unique form of innate training inhibited by ovarian-derived hormones in females.

Keywords: Myeloid lineage, macrophage metabolism, *Schistosoma mansoni*, biological sex, metabolic disease, innate training

Introduction

Cardiovascular disease (CVD) is the leading worldwide cause of mortality (Hinton et al., 2018; Roth et al., 2017). 65% of adults in the United States are diagnosed with diabetes have elevated LDL cholesterol levels or take cholesterol lowering medications, and death rates from atherosclerotic CVD are ~1.7 times higher in this population as compared to non-diabetic adults (Emerging Risk Factors et al., 2010). It is well established that in the diabetic population, obesity, and dyslipidemia are risk factors underlying these increases in mortality, while hyperglycemia is an independent risk factor (Marks and Raskin, 2000; Wong et al., 2016). Underlying conditions such as diabetes and atherosclerosis contribute to the burden of CVD in both females and males. While the incidence of CVD is markedly higher in men than in age-matched women (Opotowsky et al., 2007; Tan et al., 2010), the risk of developing CVD while diabetic is much greater in women than men (Humphries et al., 2017; Peters et al., 2014). In non-diabetic patients, females exhibit increased insulin sensitivity in comparison to males, as well as

reduced prevalence of dysglycemia and enhanced muscle glucose uptake (Cnop et al., 2003; Kim and Reaven, 2013; Moran et al., 2008; Willeit et al., 1997), suggesting sex-dependent modulations in whole body metabolism. Recent studies suggest gut microbiota contributes to sex differences in lipid metabolism (Baars et al., 2018), but the mechanisms underlying sexual dimorphism in metabolic syndrome remain poorly understood.

Previous studies have uncovered an association between a history of helminth infection and reduced prevalence of metabolic disease in humans and rodents ((Doenhoff et al., 2002; Stanley et al., 2009; Wiria et al., 2015). Specifically, infection by Schistosomes reduces cholesterol and atherosclerotic plaques (Doenhoff et al., 2002; Stanley et al., 2009), this effect has been attributed, in part, to an anti-inflammatory phenotype in macrophages (Wolfs et al., 2014) and transcriptional reprogramming of phospholipid and glucose metabolism related genes in hepatic macrophages (Cortes-Selva et al., 2018b). Moreover, it has been postulated that schistosomes have the potential to affect long term glucose metabolism in T cells (Chen et al., 2013). Accumulating evidence suggests that biological sex affects disease progression; yet the effect of Schistosomiasis on metabolic-protection in females and males it is not well understood, as most studies have been conducted only in males or no sex differentiation has been made during data analysis ((Sanya et al., 2019; Shen et al., 2015; Wolde et al., 2019)).

Schistosomiasis induces Th2 polarization and alternative activation of macrophages, essential for host survival (Barron and Wynn, 2011; Fairfax et al., 2013; Herbert et al., 2004). IL-4 induced alternative activation of macrophages relies on oxidative phosphorylation (OXPHOS) and fatty acid oxidation for energy production and is dependent on cell intrinsic lysosomal lipolysis

(Huang et al., 2014; Vats et al., 2006). Macrophage metabolism follows a dysmorphic pattern, as sex-related differences affect the processes involved in cholesterol and lipid metabolism in macrophages as well as inflammatory cytokine production in adipose tissue (Griffin et al., 2016; Ng et al., 2001). Moreover, in rats, phagocytes from females had increased ROS generation than males (Rudyk et al., 2018). Our lab recently published that *S. mansoni* infection of male mice induces a form of innate immune memory that modulates myeloid lipid and mitochondrial metabolism, while also protecting from all aspects of high fat diet induced metabolic disease. Neither this whole-body protection, nor modulation of mitochondrial metabolism occurs in schistosome infected females. Such differences have often been attributed to the role of sex hormones in gene expression and immune cell function (Rubinow, 2018; Taneja, 2018; Winn et al., 2019), but a clear understanding of the effects of sex on the regulation of macrophage metabolism, as well as how sex modulates the effects of Schistosomiasis in the protection from metabolic disease is lacking.

In the present study, we sought to determine the genetic and hormonal mechanisms of sex-dependent schistosome driven innate immune memory. We found profound biological sex driven differences in the transcriptional control of glucose and lipid metabolism, independent of infection status along with differential regulation of key genes in both glycolysis and mitochondrial metabolism by infection in males and females. Surprisingly, we found that while testes produced hormones are not necessary for infection induced protection from metabolic disease in males, elimination of ovarian derived hormones in females allows for schistosome infection to both protect from systemic metabolic disease and induce myeloid metabolic plasticity and innate immune memory. We established that schistosome egg antigens are

sufficient to induce protective innate immune training and developed an *in vitro* method for inducing metabolically protective innate immune training that enabled the finding that bone marrow from intact females can be trained *in vitro* without hormones with SEA the same way tht male bone marrow can be . Overall, these data present the first evidence that ovarian produced hormones block metabolically protective schistosome induced innate immune memory and provide a more complete understanding of how schistosome induced innate training may confer metabolic protection at the cellular level.

Results

S. mansoni infection modulates the myeloid transcriptome in a sex-specific manner

We previously documented significant sex dependent shifts in functional metabolism in BMDM from male and female *S. mansoni* infected mice(Cortes-Selva et al., 2021), we sought to determine if differential transcriptional modulation underlies these shifts. In order to investigate the genes and respective pathways that were associated with specific conditions and the ones that were differentially regulated by sex we performed mRNAseq on unstimulated BMDM derived from male and female ApoE$^{-/-}$ mice at 10-weeks post *S. mansoni* or mock infection. Comparing uninfected males to uninfected females we identified 3926 genes with adj $p<0.05$ suggesting that there are significant differences in the myeloid compartment of males and females under HFD induced metabolic conditions. Surprisingly, multiple metabolic genes that we identified in our previous publication (Cortes-Selva et al., 2021) as upregulated in males by *S. mansoni* infection are actually downregulated during metabolic disease in uninfected males compared to uninfected females, including *Hk3* (hexokinase 3) , *Mgll* (monoglyceride lipase), *Ptges* (prostaglandin E synthase), and *Slc1a3* (solute carrier family 1 (high affinity glutamate

transporter), member 3) (Figure 1A). Specifically comparing BMDM from infected males versus infected females we find that many of these genes that are more highly expressed in females than males during metabolic disease in the absence of infection, are flipped in infected animals, such that *Fabp4* (fatty acid binding protein 4), *Mgll*, *Hk3*, and *Slc1a3* are upregulated in infected males as compared to infected females. Female ApoE$^{-/-}$ mice of reproductive age are similar to female humans in that they do not get as obese or insulin resistant on HFD as male ApoE$^{-/-}$. These data suggest that the regulatory response to infection in the myeloid lineage in males and females is opposite, with males upregulating genes that may be involved in reducing the severity of disease in females, while infection in females downregulates those genes. Critically, our previous work (Cortes-Selva et al., 2021) identified that Mgll activity was needed for increased mitochondrial respiration in BMDM from infected males, as inhibition eliminated the increases in both basal and maximal respiration. We identified different subsets of genes that were preferentially upregulated in males ($p<0.05$, Supplementary Figure 1A). Among 1444 genes upregulated in males regardless of infection status with a p value <0.05, we identified histone and chromatin remodeling pathways as significantly regulated, suggesting a differential potential for epigenetic regulation in males versus females. A large subset of the 1444 genes (238 genes) were associated to metabolic functions. Of these 238 genes involved in metabolism we identified hexokinase 1 (*Hk1*), citrate synthase (*Cs*), apolipoprotein A2 (*Apoa2*), aldehyde dehydrogenase 3 family member A2 (*Aldh3a2*), lipoyltransferase (*Lipt1*), solute carrier family 19 member 1 (Slc19a1), LDL receptor related protein 1 (*Lrp1*), many of these are involved in lipoprotein and cholesterol metabolism. These data suggest that myeloid metabolism is differentially regulated by sex, at least in the context of HFD induced inflammatory environment. In addition, we found 216 genes involved in immunity. Among genes with immune function, we identified interleukin

10 (*Il-10*), Toll like receptor 5 (*Tlr5*), NLR family pyrin domain containing 3 (*Nlrp3*), inducible T cell costimulatory (*Icos*), which have diverse pro and anti-inflammatory function in the immune system. Next, we surveyed the genes that are differentially regulated in males and females following *S. mansoni* infection. We found 67 genes involved in metabolism (fatty acid and ceramide), hemostasis, the adaptive immune system, cellular migration and activation. Following the genes with known function, a large fraction of differentially regulated genes have documented roles in metabolism. Among these, we identified type II iodothyronine deiodinase (*Dio2*), which has implicated in the regulation of diet induced obesity (Kurylowicz et al., 2015; Vernia et al., 2013). Moreover, we found hexokinase 3 (*HkIII*), fatty acid binding protein 4 (*Fabp4*), sphingomyelin synthase 2 (sgms2), solute carrier family 6 member 8 (*Slc6a8*), and *Pfkb3* (6-phosphofructo-2-kinase/fructose-2,6-biphosphatase 3) were all upregulated in male and downregulated in female BMDM following *S. mansoni* infection (Figure 1C). PFKFB3 protects against diet-induced adipose tissue inflammatory responses and systemic insulin resistance in mice (Huo et al., 2012), and increased expression of *PFKFB3* is essential for suppressing adipocyte proinflammatory response by metformin (Qi et al., 2017). Importantly, lower PFKFB3 expression in subcutaneous adipose tissue has been associated with insulin resistance in women (Arner et al., 2016). HKIII is not as well studied as HKII, but hexokinase two and three are thought to have some overlapping metabolic functions (Wilson, 2003). HKII overexpression has been shown to increase ATP levels and preserve mitochondrial membrane potential, while also being associated with higher levels of transcription factors that regulate mitochondrial biogenesis, and greater total mitochondrial DNA content (Wyatt et al., 2010). We subsequently performed ATAC-seq analysis on macrophages differentiated from males and females as above. The overall read quality of the uninfected and infected groups was similar across males and

179 females (Supplementary Figure 1B). Focusing on differentially accessible regions that are
180 located around transcription start sites (TSSs), infection in males increases overall accessibility,
181 while infection in females decreases accessibility (Figure 1D), supporting the hypothesis that
182 females, in contrast to males, have an inherently different epigenetic response to schistosomes
183 that likely underlies the lack of a developing a protective metabolic reprograming in response to
184 schistosome infection.
185
186 **_S. mansoni_-increases fatty acid oxidation in male but not female ApoE$^{-/-}$ mice on HFD**
187
188 To determine whether infection-induced protection from weight gain and insulin intolerance in
189 males but not females was accompanied by sex specific differential macrophage metabolic
190 regulation, we cultured bone marrow cells from 10 week infected or uninfected control male and
191 female mice for 7 days to generate BMDM. The Oxygen consumption rate (OCR) was measured
192 in real time in basal conditions and following the addition of mitochondrial inhibitors in
193 unstimulated BMDM from both infected and uninfected male and female ApoE$^{-/-}$ animals.
194 Consistent with what we have previously published (Cortes-Selva et al., 2021), BMDM from
195 infected males exhibited increased basal OCR and spare respiratory capacity compared to
196 uninfected male controls (Figure 2A, 2B, 2C). However, basal OCR and spare respiratory
197 capacity of BMDM from infected females remained unaltered in comparison to BMDM from
198 uninfected females (Figure 2A, 2B, 2C). Moreover, side by side OCR analysis in females and
199 males with palmitate as a substrate (glucose limiting conditions) showed that BMDM from
200 infected male, but not from infected females had an increased ability to oxidize exogenous
201 palmitate (Figure 2D). In addition, BMDM from infected males but not females had significantly

increased palmitate basal OCR and palmitate spare respiratory capacity, suggesting exogenous free fatty usage as a carbon source for OXPHOS (Figure 2E, 2F). Similar to the male only data, we observed no differences in macrophage bulk neutral lipid content in either group, suggesting that global lipolysis may not underlie OCR and spare respiratory capacity in our model (Figure 2G). Additionally, analysis of mitochondrial mass via mitotracker in females and males showed BMDM from male infected mice, but not females have a significantly higher Mitotracker MFI. These data suggest that *S. mansoni* infection induces mitochondrial biogenesis in males, but not females. Again, suggesting differential regulation of macrophage metabolism based on biological sex.

S. mansoni infection differentially alters the cellular lipid profile in female and male mice

To understand the sex-specific modulations induced by Schistosomiasis in macrophage lipid metabolism, we isolated cellular lipids from unstimulated BMDM and conducted untargeted lipidomics on cells from both male and female mice. Using partial least squares discriminant analysis (PLS-DA), we discerned distinct lipid profiles associated with *S. mansoni* infection in a sex-specific manner (Figure 3A). PLS-DA is relevant as it enhances group separation by maximizing variance explained by the lipidomic data, highlighting significant differences between infected and uninfected samples. Further analysis revealed that total cholesteryl esters (CE), identified as a variable importance in projection (VIP) species in males in our previous publication (Cortes-Selva et al., 2021) decreased in cells from infected male mice but increased in BMDM from infected female mice (Figure 3B). This indicates profound sex-specific metabolic reprogramming in response to infection. Infection in females, similar to males, induces

a unique lipid signature (Figure 3C). Notably, plasmanyl-phosphatidylethanolamine (plasmanyl-PE), plasmanyl-phosphatidylcholine (plasmanyl-PC), bis(monoacylglycerol)phosphate (BMP), and CE species were the main drivers of the altered lipid profile in infected females (Figure 3D). Interestingly, BMP abundance remained unchanged by infection in males but increased significantly in females (Figure 3E), suggesting differential regulation of lipid and cholesterol metabolism pathways based on biological sex. Consistent with our previous findings, infection in males increased cellular free fatty acids, while levels remained unchanged in females. These data support the hypothesis that *S. mansoni* infection differentially modulates cellular metabolism in BMDM, with distinct metabolic adaptations in males and females.

Elimination of Ovarian hormones allows female to undergo schistosome induced innate training.

Considering the strong sex differences in both myeloid transcriptome and metabolic capacity we asked if testes derived hormones are required for protective innate immune training in male, or if ovarian derived hormones in females block schistosome induced innate training. Female ApoE$^{-/-}$ were ovariectomized and males were castrated at 5-6 weeks of age, followed by feeding of high fat diet and infection/mock infection with *S. mansoni*. Ovariectomized uninfected control mice had significantly higher glucose area under the curve and body weight than intact uninfected controls, phenocopying what often occurs after menopause or hysterectomy (Laughlin-Tommaso et al., 2018; Stachowiak et al., 2015). Surprisingly, infected ovariectomized mice had significantly lower glucose AUC than ovariectomized uninfected, intact infected and intact uninfected control females, as well as lower body weight than uninfected ovariectomized mice (Figure 4A). Castration reduces bodyweight somewhat, likely due to the known effects of

testosterone on muscle mass (Antonio et al., 1999) but does not eliminate infection induced reductions in glucose area under the curve that reflects better glucose tolerance (Figure 4B). To determine if ovariectomy allowed the same reprogramming of myeloid metabolism as seen in males, we assayed metabolic fuel source flexibility of individual carbon sources (Figure 4C). For the single-carbon substrate extracellular flux assays, data is calculated as the difference between total respiration, and respiration when the specific pathways of interest are inhibited (2-deoxyglucose for glucose, 6-diazo-5-oxo-L-norleucine for glutamine, and etomoxir for palmitate) which reflects a fraction of the total respiration levels observed from BMDM in complete media from ovariectomized infected females. The data demonstrate ovariectomy prior to schistosome infection leads to a significantly greater ability to use all three substrates (glucose, palmitate and glutamine) for cellular respiration, indicating metabolic plasticity similar to what we have published is induced by innate training in males (Cortes-Selva et al., 2021).

Egg antigen injection is sufficient to induce trained myeloid immunity and protection from metabolic disease in males

Schistosome infection induces dramatic changes to both the systemic cytokine environment and the adaptive immune compartment along with tissue damage that could alter both systemic metabolism and the bone marrow microenvironment. To validate that schistosome egg antigens (SEA) alone can recapitulate the infection induced metabolic protection we have seen in males, we placed male ApoE$^{-/-}$ mice on HFD for 4.5 weeks (to mimic the pre-egg laying period of our infection model) and then began bi-weekly injections of SEA or PBS as a vehicle control. Over the course of 5 weeks of injection, SEA slowed the HFD induced weight gain and after 5 weeks on SEA, treated mice had a 40% reduction in body fat and a 20% increase in lean mass (as

271 measured by NMR, Figure 5A) as well as a significantly lower glucose AUC (Figure 5B). We
272 then assessed whether the myeloid compartment of these mice had undergone training similar to
273 what we have demonstrated for infection by generating BMDM with MCSF in a 7-day culture.
274 BMDM from SEA injected ApoE$^{-/-}$ males have higher OCR area under the curve (Figure 5C) and
275 maximal respiration (Figure 5 D) with palmitate as a carbon source than BMDM generated from
276 control PBS injected mice. These data demonstrate that schistosome egg antigens alone can both
277 modulate whole-body metabolism and induce a unique training of the myeloid linage that
278 features an increase in fatty acid oxidation.
279
280 ***In vitro* training of bone marrow progenitors from males and females generates**
281 **macrophages with metabolic profiles like *in vivo* infection trained cells.**
282 Whole body hormonal addback experiments are challenging to use for experiments focused on
283 cellular mechanisms, so we sought to develop a method for inducing schistosome trained
284 immunity *in vitro*. Culture of bone marrow progenitors with SEA prior to macrophage
285 differentiation with MCSF (Day 0) leads to an increase in both basal and maximal respiration
286 that can be further increased in fully differentiated mature macrophages (day 7 of a 7-day
287 culture) with a 24-hour stimulation (SEA d0+24hrs) (Figure 6A, B). Our data in females strongly
288 suggested that ovarian derived hormones may directly block schistosome induced metabolically
289 protective innate training, but it is unclear if this is a chronic or acute effect of the hormones. So
290 we asked if female bone marrow myeloid progenitors could be trained by SEA in culture
291 conditions without hormones. Similar to the male data, female bone marrow trained with SEA *in*
292 *vitro* prior to macrophage differentiation has a significantly basal (Figure 6 C) and maximal
293 (Figure 6 D) OCR as compared to control untrained cells.

294

295 **SEA innate immune training increases chromatin accessibility of mitochondrial replication**
296 **and metabolic pathways in male BMDM**

297 Since we can replicate the most salient features of schistosome trained immunity with SEA
298 exposure while removing the influence of systemic inflammation, we performed ATAC-seq on
299 *in vitro* SEA trained BMDM. SEA training prior to macrophage differentiation significantly
300 alters the chromatin accessibility landscape, with lipid metabolic processes being one of the top
301 more accessible pathways (Figure 7A). We identified *Tfam* and *Ffar2* as two genes that have
302 increased chromatin accessibility within the lipid pathways. QPCR analysis showed both genes
303 have increased expression in SEA trained versus control BMDM (Figure 7B). *Ffar2* was also
304 identified in our transcriptomic analysis of BMDM from infected males (Figure 2 and (Cortes-
305 Selva et al., 2021). Ffar2 recognizes short chain fatty acids such as butyrate and has previously
306 been shown to decrease histone deacetylation levels fitting with our data that demonstrates that
307 schistosome trained immunity induces a unique epigenetic profile. Tfam is a nuclear expressed
308 mitochondrial DNA binding protein that has been shown to regulate mitochondrial membrane
309 potential, metabolism (glucose and oxidative phosphorylation, (Koh et al., 2021)) as well as
310 mitochondrial biogenesis in multiple cell types. Using TOBIAS (Bentsen et al., 2020), we
311 performed digital footprinting analysis on ATAC-seq data comparing SEA- and vehicle control
312 trained -macrophages to identify transcription factors with altered accessibility. This analysis
313 (Figure 7C) revealed significant enrichment of TFs involved in mitochondrial biogenesis,
314 metabolic regulation, and immune signaling in SEA-treated cells. Notably, *Nrf1*, a regulator of
315 *Tfam* and a key driver of mitochondrial biogenesis (Zhao et al., 2023), exhibited increased
316 accessibility in SEA-treated macrophages, supporting its role in the metabolic reprogramming

observed in schistosome-trained immunity. Additional TFs with increased accessibility included *MLX* and *MLXIPL* (Mejhert et al., 2020), which are involved in lipid and carbohydrate metabolism, as well as members of the E2F family, such as *E2F3* and *E2F4*, known to regulate cell cycle and mitochondrial function (Benevolenskaya and Frolov, 2015). We then compared the TF footprint of infection in females to that of *in vitro* SEA trained male cells. Looking at the most divergent motifs between SEA trained males and infected females, we find the transcription factors we identified in males that regulated mitochondria and cell cycle in Figure 7 C such as *NRF-1* and *E2F4* are uniquely enriched in SEA trained males and not infected females. Motifs that are uniquely enriched for binding in infected females include *Hnf4a*, which can regulate lipid and carbohydrate metabolism (Huck et al., 2021), and *HOXA3* which has been shown to regulated macrophage polarization (Al Sadoun et al., 2016). *MLX* and *MLXIPL* are enriched in both groups compared to their respective controls indicating that they are likely a response to schistosome egg antigens that is unrelated to the metabolic phenotype of enhance mitochondrial respiration. These findings suggest that SEA exposure prior to male macrophage differentiation induces a coordinated epigenetic and transcriptional program to enhance mitochondrial biogenesis and metabolic flexibility.

Schistosome trained immunity increases mitochondrial number in males.

Our previous publication that defined schistosome induced innate immune training demonstrated a consistent increase in mitotracker MFI in BMDM from infected males but not females (Figure 2H and (Cortes-Selva et al., 2021)), suggesting that this form of innate immune training may induce mitochondrial biogenesis. To formally evaluate this possibility, we performed electron microscopy (EM) of BMDM generated form the bone marrow of infected and uninfected male and female ApoE$^{-/-}$ mice on HFD. BMDM generated from infected males have a greater number

of mitochondria per μm^2 than control BMDM generated from uninfected males (Figure 8 A, B). Similar to the transcriptional and lipidomic data, schistosome infected females have the opposite phenotype, with fewer mitochondria per μm^2 than control BMDM from uninfected females. Since our data demonstrated that both *in vivo* SEA injection and in vitro SEA training induces a similar metabolic phenotype, we performed EM of BMDM generated from males injected with SEA for 5 weeks and trained *in vitro* in our culture method. Both BMDM generated from SEA injected males (Figure 8E, F) *in vitro* trained BMDM (Figure 8G, H) and have significantly more mitochondria per μm^2 than control BMDM. Definitively demonstrating that schistosome training of the myeloid lineage involves increases in mitochondrial number and activity.

Discussion

Helminth infections in general, and Schistosomiasis in specific, have been known to inversely correlate with obesity and glucose intolerance for over a decade, a phenomenon thought to be associated with Type 2 polarization of macrophages and T cells. A cohort in China where Schistosomiasis was recently eradicated, demonstrated that a historical *Schistosoma japonicum* infection is associated with lower prevalence of metabolic syndrome and diabetes (Chen et al., 2013; Shen et al., 2015). There, HbA1c and insulin resistance, as well as triglyceride and LDL levels, were inversely associated with previous *Schistosome* infection, suggesting that not only does active helminth infection modulate metabolic disease, but helminths may induce long-term protection from systemic metabolic disease. Much of the published work of helminth infections and metabolism has focused on males. Our recent study was the first to demonstrate that schistosome infection induces a unique form of innate immune

362 training focused on increased mitochondrial fatty acid oxidation, and that biological sex has a
363 clear effect on the ability of the myeloid lineage to be trained *in vivo* (Cortes-Selva et al., 2021).
364 Our previous work established that in males, the hallmark of schistosome induced innate
365 training is the generation of a hybrid macrophage that is neither fully polarized to M1 or M2,
366 with decreased production of IL-6 and chronic mediators of inflammation but enhanced
367 transcription of antimicrobial genes and inos. This unique anti-inflammatory phenotype occurs
368 with increased cellular respiration and metabolic plasticity to use multiple carbon sources for
369 fatty acid oxidation respiration. At the cellular lipid level, the hallmark of these cells is
370 dramatically increased free fatty acids with decreased cholesterol esters, TAGs and DAGs. This
371 phenotype appears to be a unique form of innate immune training, as neither BCG nor β-glucan
372 increase fatty acid oxidation, and the hallmark of those forms of trained immunity in increased
373 inflammation, IL-6 and glycolysis (Arts et al., 2016). The long-lived natures of both BCG and β-
374 glucan trained immunity are enforced via epigenetic rewiring of bone marrow progenitors, with
375 BCG and β-glucan inducing enrichment of H3K4me3 at the promoters of IL6 and TNF, and
376 BCG additionally enriching H3K9me3 (Arts et al., 2016). IL-6 production/secretion is enhanced
377 in both BCG and β-glucan innate training neither of which are known to be metabolically
378 protective. Intriguingly, *Dnmt1*, involved in DNA methylation maintenance (Hervouet et al.,
379 2018), is downregulated in males but remains statistically unchanged in females in our
380 transcriptomic analysis following infection. While *Dnmt3a*, essential for establishing DNA
381 methylation patterns during development and implicated in hematopoietic stem cell clonal
382 expansion (Wang et al., 2024), is upregulated in males but downregulated in females (Figure 1).
383 These data support the hypothesis that sex-specific differences in the regulatory epigenetic
384 landscape underlie the protective metabolic reprogramming observed in males but not females.

In our model the most direct comparison for alterations to the chromatin landscape between schistosomes and β-glucan would be the ATACseq data from *in vitro* SEA trained BMDM. A large percentage of the regions with increased accessibility are related to mitochondrial function and cell cycle, which have not been reported for either BCG or β-glucan. Indeed, one of the transcription factors that is enriched from the TOBIAS analysis is Nrf1, which regulates *Tfam* expression and pathways related to mitochondrial respiratory function (Satoh et al., 2013). We validated that *Tfam* transcript is indeed upregulated in these cells (Fig 7). Tfam has been shown to increase hexokinase activity (Koh et al., 2019), so we hypothesize that the combined effects of epigenetically upregulating *Nrf1* and *Tfam* are key components of metabolically protective schistosome induced innate training. Critically, *Nrf-1* and *E2f* family motif enrichment does not occur in infected females (Figure 7 D), which do not have increases in number of mitochondria or in mitochondrial respiration.

We have previously hypothesized that schistosome induced training increases mitochondrial respiration in males via mitochondrial biogenesis, but that hypothesis was based only on flowcytometric quantitation of mitotracker staining. In this current study we performed electron microscopic imaging of BMDM generated from infected and control males and females and found that BMDM from infected males have increased mitochondria per area compared to control uninfected, while females have fewer mitochondria. Additionally, on the 2000x images it appears that BMDM from infected females may have more small lipid bodies, although we have not formally quantified that, future work will focus on these sex specific ultrastructure differences. Since schistosome infection induces systemic inflammation and increase to many cytokines, we utilized *in vitro* and *in vivo* SEA exposure to determine if the increase in mitochondria in male BMDM were directly driven by schistosome antigens. BMDM from both

training conditions demonstrate increased mitochondria, with the most dramatic increases in the culture trained BMDM, definitively indicating that SEA training of the myeloid lineage induces mitochondrial biogenesis.

In the current study we report that schistosome infection differentially regulates the transcriptome, chromatin landscape, and mitochondrial metabolism in males and females and that schistosome egg antigens exposure can replicate this unique innate immune training *in vivo* and *in vitro*. Analysis of the BMDM transcriptomes from males and females revealed that over a thousand genes are upregulated in male versus female BMDM regardless of *S. mansoni* infection state. Hundreds of these are annotated to metabolic pathways, suggesting that there are inherent differences in male and female myeloid cellular metabolism. Over five dozen are differentially regulated by infection. Focusing on the genes that are upregulated in BMDM from infected males and downregulated in females, we found more than ten genes with known functions in cellular metabolism. Some of these genes, like *PFKFB3*, have known regulatory elements for progesterone and estrogen, but some of them, like *Fabp4*, have no published mechanism of sex hormone regulation. Hexokinase transcripts are elevated in males and either not changed (*Hk1*) or downregulated (*Hk3*) in females. Estrogen has been documented to regulate hexokinase enzyme activity (but not transcription) in some cell types via activation of the Akt pathway (Brinton, 2008). It is unclear if that occurs during schistosome infection as glycolysis is not significantly increased in infected females. Our previously published data indicates that for males, the upregulation of glycolysis is to generate TCA cycle intermediates and not lactate as an end product (Cortes-Selva et al., 2021), so the regulation induced by infection may be distinct from other models. Our data from ovariectomized and castrated mice demonstrate that the sex difference is most likely driven by an inhibitory effect of ovarian derived hormones, as castration

of males does not prevent schistosome induced training, but ovariectomy of females renders them permissive to schistosome induced training. Indeed, our culture-based method of inducing schistosome innate training demonstrates that in culture conditions where physiological levels of female hormones are absent, female bone marrow can generate trained BMDM with increased mitochondrial respiration levels similar to males. Combined with our ATAC-seq data showing that infection increases chromatin accessibility in males and decreases it in females (Fig 1), there is strong support for the hypothesis that female hormones inhibit schistosome induced training at the progenitor level.

At the whole-body level there are known differences in lipid and glucose metabolism between males and females, with females generally having more body fat (higher subcutaneous and lower visceral) as well as lower muscle mass. The regulation of the distribution of body fat has been attributed to estrogen, as deposition shifts from subcutaneous to visceral after menopause (Svendsen et al., 1995) and deletion of estrogen receptor in mice leads to less subcutaneous adiposity (Lapid et al., 2014). Additionally, women tend to have higher non-oxidative free fatty acid clearance via re-esterification than men (Nielsen et al., 2003), suggesting that women tend to store fatty acids from the circulation while men oxidize them. At the myeloid level, males on high fat diet have increased myelopoiesis compared to females, as well as more proinflammatory adipose tissue macrophages (Singer et al., 2014). These differences are hormonally regulated as castration of males in this model reduces adipose monocyte inflammation while ovariectomy of females increased adipose tissue macrophages and bone marrow myeloid colony formation (Varghese et al., 2021). Very few studies have focused on sex differences in myeloid cellular lipid or glycolytic metabolism but comparing the uninfected control male and female lipidomics in figure 3, females have a higher abundance of free fatty

454 acids in addition to multiple PE and PC species than males. While our 2018 publication (Cortes-
455 Selva et al., 2018a) did not include females, the liver macrophage transcriptomic data suggested
456 similar shifts in male myeloid cellular metabolism as we have described in BMDM in both this
457 current paper and our 2021 paper (Cortes-Selva et al., 2021). Taking all these data together, the
458 scientific premise that there is a flip in storage versus usage of lipids and free fatty acids in male
459 and female macrophages that is amplified in the context of schistosome induced innate immune
460 training is well supported. Additional studies are needed to determine if our BMDM data is
461 representative of adipose and other tissue macrophage population during metabolic disease in
462 males versus females and if schistosome induced innate training similarly drives fatty acid
463 oxidation in metabolic tissues.

464 There are significant differences in both the susceptibility to disease presentation of
465 diabetes and CVD between males and females, with females having lower rates of diabetes but
466 increased risk of cardiovascular complications once diabetic (Humphries et al., 2017; Peters et
467 al., 2014; Yoshida et al., 2023). Few studies have focused on the role of immunometabolism in
468 this dichotomy. Females of reproductive age are generally protected from severe metabolic
469 disease compared to similarly obese males (Li et al., 2022). This protection goes away post-
470 menopause (Heianza et al., 2013), suggesting that ovarian derived hormones are involved. Data
471 from cancer, type 1diabetes, and reproductive studies indicates that progesterone can modulate
472 whole body and tissue/cellular glucose metabolism (Atif et al., 2019; Picard et al., 2002) with
473 sometimes conflicting results (Lee et al., 2020; Lee et al., 2018). Estradiol can both bind directly
474 to fatty acids and induce a form of lipolysis, while also increasing glucose uptake *in vitro*, and
475 hepatic gluconeogenesis *in vivo* in some models (Yan et al., 2019). Estradiol replacement therapy
476 in post-menopausal women lowered blood glucose and increased insulin sensitivity in some

studies (Friday et al., 2001), while others found an increasing risk of type 2 diabetes with increasing duration of postmenopausal estrogen use (Zhang et al., 2002). Our data suggests clear biological sex differences driven by ovarian derived hormones in both the ability of schistosomes to protect from the development of HFD induced metabolic disease parameters, and the ability of schistosome antigens to train the myeloid lineage towards a protective phenotype via mitochondrial biogenesis and increased respiration. There are limitations to our current model, as SEA contains hundreds of proteins as well as carbohydrates and lipids. Future work will be focused on determining what components of SEA are necessary and sufficient to induce the metabolically protective innate training described in this study. Our current data also indicate a clear need for further studies in both humans and animal models to specifically probe the relationship between biological sex and myeloid metabolism, and how various steroid hormones regulate both cellular and whole-body metabolism.

Figure Legends

Figure 1. ***S. mansoni*** **infection modulates the myeloid transcriptome in a sex-specific manner**

ApoE$^{-/-}$ mice were fed HFD diet for 10-days before infection/mock infection with *S. mansoni*. Bone marrow was harvested at 10-weeks post infection, and BMDM were differentiated with M-CSF. RNA-seq and ATAC-seq was performed on cells from separate cohorts of mice. A) Volcano plot of Genes upregulated in control uninfected ApoE$^{-/-}$ males on HFD versus control uninfected females. B) Volcano plot of Genes upregulated by infection in ApoE$^{-/-}$ males on HFD versus infected females. C) Overlap of genes significantly upregulated by *S. mansoni* infection in males and those downregulated by infection in females (adjusted p-value <0.05) along with pathway analysis of the 67 differentially regulated genes. The gene list is in supplementary

Table .1 D) Heatmap of peaks that are significantly altered by infection near transcription start sites from the ATAC-seq data of each sex. RNA Sequencing data are from one experiment with 4-5 mice per group, ATAC-seq data are from one experiment of 3-4 mice per group.

Figure 2. *S. mansoni* increases fatty acid oxidation in male but not female ApoE$^{-/-}$ mice on HFD

Male and female ApoE$^{-/-}$ mice were fed HFD for 10 days before infection with *S. mansoni*. At 10-weeks post infection mice were sacrificed and Mϕ were differentiated from bone marrow with M-CSF. A) SeaHorse assay results for OCR of BMDM from infected and uninfected ApoE$^{-/-}$ males and females in complete media in basal conditions and in response to mitochondrial inhibitors. (B) Quantification (in picomoles/minute) of the basal oxygen consumption of BMDM. (C) Quantification of the spare respiratory capacity of BMDM from A. D) SeaHorse assay results for OCR of BMDM from infected and uninfected ApoE$^{-/-}$ males and females in media where palmitate is the carbon source in basal conditions and in response to mitochondrial inhibitors. E) Quantification (in picomoles/minute) of the basal oxygen consumption of BMDM from D. F) Quantification of the spare respiratory capacity of BMDM from D. G) Oil Red O relative staining in BMDM. H) MitoTracker Red Deep Stain measured by flow cytometry in BMDM.

Figure 3. *S. mansoni* infection differentially alters the cellular lipid profile in female and male mice

BM was harvested as above and Mϕs were differentiated with M-CSF in a 7-day culture. Total cellular lipids were extracted and analyzed via LC-MS based lipidomic analysis. A) PLS-DA derived score from Female and Male HFD Infected BMDM. B) Box whisker plot of normalized

AUC of cholesterol ester species, between female infected and uninfected ApoE$^{-/-}$ mice on HFD. C) PLS-DA derived score from HFD infected and HFD uninfected female BMDM. D) Volcano plot identifying VIP lipids in infected females. E,F) Box whiskers plots (10–90 percentile) of relative abundance of normalized BMPs and all species of free fatty acids, data are normalized to sum and treated with pareto scaling, each dot is a single species. Data are representative of 3 experiments with 4–6 mice per group in each experiment.

Figure 4. **Elimination of Ovarian hormones allows female to undergo schistosome induced innate training.**

Male and female ApoE$^{-/-}$ mice were gonadectomized at 5.5 weeks of age and then fed HFD for 10 days before infection with *S. mansoni* controls are left intact. At 10-weeks post infection body weight and glucose tolerance were measured prior to sacrifice (A,B). C) Mϕ were differentiated from bone marrow from females in the indicated groups with M-CSF. Maximal respiration for individual carbon sources (Glucose, Glutamine, and Palmitate) measured at steady state in single carbon substrate media and specific inhibitors for each pathway. Data are representative of 3 experiments with 5-6 mice per group in each experiment. Statistical significance calculated using ANOVA.

Figure 5. **Egg antigen injection is sufficient to induce trained myeloid immunity and protection from metabolic disease in males**

Male ApoE$^{-/-}$ mice were fed HFD for 4 weeks before bi-weekly injections of SEA for 5 weeks. A) Body weight was measured biweekly at the start of SEA administration. B) At 9 weeks post HFD, 5 weeks post SEA- body composition was measured using NMR and a glucose tolerance test was performed. C) SeaHorse assay results for OCR of BMDM from PBS and SEA injected

ApoE$^{-/-}$ males in media where palmitate is the carbon source in basal conditions and in response to mitochondrial inhibitors. Data are representative of 2 experiments with 4-5 mice per group in each experiment. Statistical significance calculated using t- tests.

Figure 6. ***In vitro*** **training of bone marrow progenitors from males and females generates macrophages with metabolic profiles similar to infection trained cells**

Male and female ApoE$^{-/-}$ mice were fed HFD for 6 weeks before bone marrow was harvested. Bone marrow was exposed to SEA (SEA d0) or just media (No SEA) prior to differentiation of macrophages with M-CSF. At day 7 of differentiation, cells from SEA d0 were split and stimulated with either media or SEA for 24hr (d0+SEA 24hs). SeaHorse assays were performed in complete media. A, C) Quantification (in picomoles/minute) of the basal oxygen consumption of BMDM. B,D) Quantification (in picomoles/minute) of the maximal oxygen consumption of BMDM. Statistical significance calculated using ANOVA data are representative of at least 3 biologically independent experiments.

Figure 7. **SEA innate immune training increases chromatin accessibility of mitochondrial replication and metabolic pathways**

Male ApoE$^{-/-}$ mice were fed HFD for 6-8 weeks before bone marrow was harvested. Bone marrow was trained *in vitro* as described in figure 6 with SEA or PBS control followed BMDM differentiation with MCSF. At day 7 of differentiation nuclei were extracted from cells and ATAC-seq was performed. A) Pathway enrichment analysis of differentially accessible peaks reveals in SEA-trained BMDMs compared to PBS controls. B) Relative transcript abundance of *Tfam* and *Ffar2* quantified by RT-qPCR. Statistical significance was determined using t- tests. C) TOBIAS footprinting analysis of ATAC-seq data identifies TFs with enriched binding activity in

SEA-trained BMDMs. D) 4-way scatterplot of the most divergent TF motifs between SEA trained male cells and infected females.

Figure 8. **Schistosome trained immunity increases mitochondrial number in males.** BMDM were generated as for each condition as described in previous figure. BMDM were fixed with 2.5% glutaraldehyde and 1% paraformaldehyde, processed for embedding in resin, sectioned and then stained with uranyl acetate. Mitochondria were quantified using ImageJ in 1000X images that contained 1-3 macrophages per image. Representative images are 2000x. A, B) BMDM generated from male control and infected ApoE$^{-/-}$ mice on HFD at 10 weeks post infection. C, D) BMDM generated from female control and infected ApoE$^{-/-}$ mice on HFD at 10 weeks post infection E, F) *In vivo* trained SEA Male ApoE$^{-/-}$ mice were fed HFD for 4 weeks before bi-weekly injections of SEA for 5 weeks. G, H) *In vitro* SEA trained ApoE$^{-/-}$ BMDM as described in Fig 6. Statistical significance calculated using t- tests.

Conflict of Interest

The authors declare no competing interests.

Acknowledgements

KCF and EA conceived of the project; KCF, EA, JEC, JMO, and DCS designed the experiments; KCF, DCS, LG, EA, and JAM, performed the experiments; KCF, DCS, EA, JAM, JEC, and SF analyzed the data; KCF, DCS, and JMO wrote the manuscript. The work was supported by The University of Utah, a Scientist Development Grant from the American Heart Association to KCF (14SDG18230012), 1 R01 AI158710-01 to KCF and EA, an American Heart Association Pre-doctoral Award (18PRE34030086) to DCS, and 1R21AI135385-01A1 to EA. *B. glabrata* snails provided by the NIAID Schistosomiasis Resource Center of the Biomedical Research Institute (Rockville, MD) through NIH-NIAID Contract HHSN272201700014I for distribution through BEI Resources. JEC is supported through U54 DK110858-01, mass spectrometry equipment employed was provided by 1S10OD016232-01, 1S10OD018210-01A1 and 1S10OD021505-01 to JEC.

LEAD CONTACT AND MATERIALS AVAILABILITY

Further information requests should be directed to and will be fulfilled by the Lead Contact, Keke Fairfax (keke.fairfax@path.utah.edu). These studies generated no new reagents.

EXPERIMENTAL MODEL AND SUBJECT DETAILS

Ethics statement

This study was carried out in accordance with the recommendations in the Guide for the Care and Use of Laboratory Animals of the National Institutes of Health. The protocols were approved by the Institutional Animal Care and Use Committees of the University of Utah (#18–09001).

Parasite and mouse models

Snails infected with *S. mansoni* (strain NMRI, NR-21962) were provided by the Schistosome Research Reagent Resource Center for distribution by BEI Resources, NIAID NIH. ApoE$^{-/-}$ (B6.129P2-Apoetm1Unc/J) were purchased from the Jackson Laboratories and bred at the University of Utah. Castration and Ovariectomy or sham-operation were performed by Jax surgical services. 6-8-week-old male mice were housed in pathogen-free conditions and were fed standard rodent chow (2019 rodent chow, Harlan Teklad) until 10–14 days before infection when they were transitioned to a high-fat diet (HFD: 21% milk fat, 0.15% cholesterol: TD 88137 Envigo).

S. mansoni infection and glucose tolerance test

623 ApoE$^{-/-}$ male mice of 6 weeks of age were exposed percutaneously to 75–90 cercariae
624 of *S. mansoni* or were mocked infected (as controls). At five- and ten-weeks post-infection mice
625 were fasted for four hours and baseline blood glucose levels were obtained via lateral tail vein
626 nick. Mice were then administered a single intraperitoneal injection of glucose (2mg/g of body
627 weight, ultrapure glucose, Sigma G7528). Blood glucose levels were obtained at 20, 60, and 90-
628 minutes post injection. Individual data points obtained were analyzed by Area Under Curve
629 (AUC).
630
631 **SEA injections**
632 Male or female ApoE$^{-/-}$ of 6 weeks were on HFD for 4 weeks. After that, mice were injected
633 biweekly with 50 ug of SEA or PBS as negative control and weight variation measured. After 5
634 weeks of injections, an IP glucose tolerance test was performed (Cortes-Selva et al., 2021). Body
635 weight and fat were measured using a Bruker Minispec LF50 device (Bruker, Karlsruhe,
636 Germany). Finally, bones were collected for cultures to generate BMDM.
637
638 **Mouse macrophage culture**
639 Mouse bone marrow-derived macrophages (BMDM) were generated as follows: bone marrow
640 cells were isolated by centrifugation of bones at >10,000 x g in a microcentrifuge tube for 15
641 seconds as previously described [76]. Cells were differentiated in M-CSF (20ng/mL, Peprotech,
642 Rocky Hill, NJ) in complete macrophage medium (CMM: RPMI1640, 10% FCS, 2mM L-
643 glutamine and 1 IU/mL Pen-Strep for 6 or 7 days. On the last day, cells were harvested in
644 Cellstripper cell dissociation reagent (Corning) were washed with CMM and prepared for
645 downstream assays. For generation of ex vivo SEA trained macrophages, 5ug/ml of SEA was

added to the complete media culture with the bone marrow cells at (d0), for stimulation of mature macrophages, the same amount of SEA was added at d6. When the effect of sexual hormones was tested charcoal stripped Fetal Bovine serum (Gibco, Qualified One shot) and media without phenol red were used.

Flow cytometry

Staining of BMDM was performed using the following mAb against mouse antigens: F4/80 (BM8, Biolegend), Mitotracker DeepRed (ThermoFisher), and Oil RedO (Thermo Fisher) . Samples were acquired using Attune NxT Focusing Flow Cytometer (Thermo Fisher Scientific) and analyzed using Flowjo X 10.10.0 (FlowJo LLC, Inc.).

Glycolytic and phospho-oxidative metabolism measurement (seahorse assay)

BMDM from different conditions were resuspended at the same concentration in XF assay media supplemented with 5% FCS and 5mM glucose. The day before the assay, the probe plate was calibrated and incubated at 37 C in a non-CO2 incubator. Resuspended cells were seeded at a concentration of $1.5x10^5$ cells per well and incubated for 20-60 minutes in the Prep Station incubator (37 C non-CO2 incubator). Following initial incubation, XF Running Media (XF assay media with 5% FCS and 10mM Glucose) were dispensed into each well. OCR and ECAR were measured by an XF96 Seahorse Extracellular Flux Analyzer following the manufacturer's instructions. For the seahorse assay, cells were treated with oligomycin (1uM), FCCP (1.5uM), rotenone (100nM) and antimycin A (1uM). Each condition was performed in 2-3 technical replicates. For determination of palmitate dependent respiration, BSA-conjugated palmitate (BSA: palmitate = 1:6, molar ratio) was prepared according to the Seahorse protocol (Seahorse Bioscience). Briefly, 1 mM sodium palmitate (Sigma Aldrich) was conjugated with 0.17 mM

669 fatty acid free-BSA (Sigma Aldrich) in 150 mM NaCl solution at 37°C for 1h. Palmitate-BSA
670 was stored in glass vials at -20°C until use. Cells were incubated as above in glucose limited XF
671 media per manufacturer instructions.

672

673

674 **RNA Isolation and q-RT-PCR**

675 BMDM were washed with PBS and then lysed with 350 ul of LBP (Takara). Then, Nucleospin
676 RNA plus kit (Takara) was used to extract RNA following manufacturer instructions. Next,
677 cDNA was synthesized from RNA using Superscript IV VILO (ThermoFisher Scientific) for
678 reverse transcription. qPCR was performed using TaqMan Gene expression assays (mgll, slc1a3,
679 beta actin, ThermoFisher) on an Applied Biosystems Stepone Plus Real-Time PCR System.
680 Beta-Actin assay number Mm02619580_g1, Tfam assay Mm00447485_m1, Ffar2 assay
681 Mm02620654_s1. Relative expression was calculated using the 2-ΔΔCt method (Arocho et al.,
682 2006).

683 **RNA Sequencing**

684 The sequencing data were first assessed using FastQC (Babraham Bioinformatics) for quality
685 control. Then all sequenced libraries were mapped to the mouse genome (UCSC mm10) using
686 STAR RNA-seq aligner [77] with the following parameter: "—outSAMmapqUnique 60". The
687 reads distribution across the genome was assessed using bamutils (from ngsutils) [78]. Uniquely
688 mapped sequencing reads were assigned to mm10 refGene genes using featureCounts (from
689 subread) [79] with the following parameters: "-s 2 –p–Q 10". Quality control of sequencing and
690 mapping results was summarized using MultiQC (Ewels et al., 2016). Genes with read count per
691 million > 0.5 in more than 2 of the samples were kept. The data was normalized using trimmed

mean of M values method. Differential expression analysis was performed using edgeR (Robinson et al., 2010). False discovery rate was computed from p-values using the Benjamini-Hochberg procedure. Pathway analysis was performed on $\log_2$-transformed data using Bonferroni-corrected *p*-values. The data discussed in this publication have been deposited in NCBI's Gene Expression Omnibus (Edgar et al., 2002) and are accessible through GEO Series accession number GSE144447 (https://www.ncbi.nlm.nih.gov/geo/query/acc.cgi?acc=GSE144447).

ATAC-seq

BMDM were treated with lysis buffer with digitonin to extract nuclei. Then, approximately 50000 nuclei were used for tagmentation following manufacturer's instructions (Diagenode), DNA purified, and libraries were prepared. After QC, libraries were sequenced using novogene service using NovaSeq 6000. Raw sequencing reads were pre-processed by trimming adapters and removing low-quality reads with TrimGalore (0.6.10) prior to alignment to the mouse genome (GRCm39.113) using BWA (0.7.17). After alignment duplicate reads and mitochondrial reads were removed. Chromatin accessibility peaks were called using MACS2 (2.2.9.1) with a q-value cutoff of 0.01. The resulting peaks were processed with BEDTools (2.31.1) to create a consensus set, then annotated to the nearest genes using HOMER (4.11). Peak reads were counted using featureCounts from the Subreads software package (2.0.6), then counts were used for differential accessibility analysis using the R package DESeq2 (1.42.1). For pathway enrichment analysis, genes were first filtered by removing those with discordant associated peaks (*i.e.* genes having both opened and closed peaks). For bias correction and transcription factor

715 footprinting, we applied TOBIAS to the ATAC-seq data (Bentsen et al., 2020). Footprint scores
716 were calculated using TOBIAS ScoreBigwig and differential motif binding was analyzed using
717 TOBIAS BINDetect and JASPAR 2022 motif libraries to estimate TF binding activities. ATAC-
718 seq data will be deposited in GEO, accession number available at publication.
719
720 **Untargeted Lipidomics Workflow**
721 *Sample extraction from serum or cell pellets*
722 Lipids are extracted from serum (50uL) or cell pellets in a combined solution as described in
723 (Matyash et al., 2008). Samples were incubated with 225 µL methanol (MeOH) containing
724 internal standards (IS; Avanti Splash Lipidomix, 10 µL per sample) and 750 µL methyl tert-butyl
725 ether (MTBE). The samples were sonicated for 1 minute, rested on ice for 1 hour with brief
726 vortexing every 15 minutes, followed by the addition of 200 µL double-distilled water (ddH_2O)
727 to induce phase separation. The samples were then vortexed for 20 seconds, rested at room
728 temperature for 10 minutes, and centrifuged at 14,000 g for 10 minutes at 4°C. The upper
729 organic phase was collected and evaporated to dryness under vacuum. Lipid samples were
730 reconstituted in 200 µL isopropanol (IPA) and transferred to an LC/MS vial with insert for
731 analysis. A process blank sample and a pooled quality control sample (10 µL per sample) were
732 also prepared.
733
734 *LC-MS Methods*
735 Lipid extracts were separated on a Waters Acquity UPLC CSH C18 1.7 µm 2.1 x 100 mm
736 column maintained at 65°C, connected to an Agilent HiP 1290 Sampler, Agilent 1290 Infinity
737 pump, and Agilent 6530 Accurate Mass Q-TOF dual ESI mass spectrometer. For positive mode,

the source gas temperature was set to 225°C, with a gas flow of 11 L/min and a nebulizer pressure of 50 psig. For negative mode, the source gas temperature was set at 325°C, with a drying gas flow of 12 L/min and a nebulizer pressure of 30 psig. Samples were analyzed in a randomized order in both positive and negative ionization modes in separate experiments, acquiring with the scan range m/z 100-1700. Mobile phase A consisted of acetonitrile:water (60:40 v/v) with 10 mM ammonium formate and 0.1% formic acid, and mobile phase B consisted of isopropanol:acetonitrile:water (90:9:1 v/v) with 10 mM ammonium formate and 0.1% formic acid. The chromatography gradient started at 15% mobile phase B, increased to 30% B over 2.4 minutes, then to 48% from 2.4-3.0 minutes, followed by an increase to 82% B from 3-13.2 minutes, and then to 99% from 13.2-13.8 minutes, where it was held until 15.4 minutes before returning to the initial condition and equilibrating for 4 minutes. The flow rate was 0.4 mL/min throughout, with an injection volume of 5 µL for positive mode and 7 µL for negative mode. Tandem mass spectrometry was conducted using the same LC gradient at collision energies of 20 V and 40 V.

Data Analysis and Pretreatment

Pooled quality control (QC) samples and process blanks were injected throughout the sample queue to ensure the reliability of the acquired lipidomic data. Results from LC-MS experiments were collected using Agilent Mass Hunter (MH) Workstation and analyzed using the software packages MH Qual, MH Quant (Agilent Technologies, Inc.), and LipidMatch (Koelmel et al., 2017) to prepare the data set. The data table exported from MH Quant was evaluated using Excel, where initial lipid targets were parsed based on the following criteria: only lipids with a relative standard deviation (RSD) of less than 30% in QC samples were used for data analysis.

Additionally, targets identified in blanks or double blanks at significant amounts (area under the curve (AUC) target blank/AUC target QC >30%) were removed from analysis.

Electron Microscopy Imaging

BMDMs were washed with PBS and fixed using Fixatives solutions (Electron Microscopy Sciences) overnight, stored at 4°C in fixative solution and sent to the Electron Microscopy Laboratory at University of Utah for further processing.

After postfixation with 2% osmium tetroxide and prestaining with uranyl acetate, the ventricular tissue slices were dehydrated in graded ethanol and pure acetone, imbedded with epoxy resin, and sectioned at 70 nm using an ultramicrotome (Leica). Sections were poststained with acetate and lead citrate before imaging with JEM-1400Plus or JEM1200-EX (JEOL) transmission electron microscope with a CCD Gatan camera.

)Samples were then dehydrated using a graded ethanol series and embedded in Embed 812 (Electron Microscopy Sciences) using a graded resin and propylene oxide series. The 1-µ transverse sections were cut with a diamond knife ultramicrotome and imaged using a Jeol 1400-plus transmission electron microscope (Jeol, Tokyo, Japan) with a high-resolution digital camera (AMT, Woburn, MA, USA). Images were captured at 1000 and 2000x for counting mitochondria and for representative images for publication. Mitochondria were counted in ImageJ.

Statistical Analysis

Statistical analyses of data were performed using one-way ANOVA, a non-parametric Mann-Whitney test, or unpaired Student's t-test depending on the data distribution. $P \leq 0.05$ were considered statistically significant. Analyses and graphing were performed using Prism (GraphPad v10.0) and R-language for statistical computing.

References

Al Sadoun, H., M. Burgess, K.E. Hentges, and K.A. Mace. 2016. Enforced Expression of Hoxa3 Inhibits Classical and Promotes Alternative Activation of Macrophages In Vitro and In Vivo. *J Immunol* 197:872-884.

Antonio, J., J.D. Wilson, and F.W. George. 1999. Effects of castration and androgen treatment on androgen-receptor levels in rat skeletal muscles. *J Appl Physiol (1985)* 87:2016-2019.

Arner, P., A.S. Sahlqvist, I. Sinha, H. Xu, X. Yao, D. Waterworth, D. Rajpal, A.K. Loomis, J.M. Freudenberg, T. Johnson, A. Thorell, E. Naslund, M. Ryden, and I. Dahlman. 2016. The epigenetic signature of systemic insulin resistance in obese women. *Diabetologia* 59:2393-2405.

Arocho, A., B. Chen, M. Ladanyi, and Q. Pan. 2006. Validation of the 2-DeltaDeltaCt calculation as an alternate method of data analysis for quantitative PCR of BCR-ABL P210 transcripts. *Diagnostic molecular pathology : the American journal of surgical pathology, part B* 15:56-61.

Arts, R.J.W., A. Carvalho, C. La Rocca, C. Palma, F. Rodrigues, R. Silvestre, J. Kleinnijenhuis, E. Lachmandas, L.G. Goncalves, A. Belinha, C. Cunha, M. Oosting, L.A.B. Joosten, G. Matarese, R. van Crevel, and M.G. Netea. 2016. Immunometabolic Pathways in BCG-Induced Trained Immunity. *Cell Rep* 17:2562-2571.

Atif, F., S. Yousuf, C. Espinosa-Garcia, E. Sergeeva, and D.G. Stein. 2019. Progesterone Treatment Attenuates Glycolytic Metabolism and Induces Senescence in Glioblastoma. *Sci Rep* 9:988.

Baars, A., A. Oosting, M. Lohuis, M. Koehorst, S. El Aidy, F. Hugenholtz, H. Smidt, M. Mischke, M.V. Boekschoten, H.J. Verkade, J. Garssen, E.M. van der Beek, J. Knol, P. de Vos, J. van Bergenhenegouwen, and F. Fransen. 2018. Sex differences in lipid metabolism are affected by presence of the gut microbiota. *Sci Rep* 8:13426.

Barron, L., and T.A. Wynn. 2011. Macrophage activation governs schistosomiasis-induced inflammation and fibrosis. *European journal of immunology* 41:2509-2514.

Benevolenskaya, E.V., and M.V. Frolov. 2015. Emerging links between E2F control and mitochondrial function. *Cancer research* 75:619-623.

Bentsen, M., P. Goymann, H. Schultheis, K. Klee, A. Petrova, R. Wiegandt, A. Fust, J. Preussner, C. Kuenne, T. Braun, J. Kim, and M. Looso. 2020. ATAC-seq footprinting unravels kinetics of transcription factor binding during zygotic genome activation. *Nat Commun* 11:4267.

821 Brinton, R.D. 2008. Estrogen regulation of glucose metabolism and mitochondrial function:
822 therapeutic implications for prevention of Alzheimer's disease. *Adv Drug Deliv Rev*
823 60:1504-1511.
824 Chen, Y., J. Lu, Y. Huang, T. Wang, Y. Xu, M. Xu, M. Li, W. Wang, D. Li, Y. Bi, and G. Ning. 2013.
825 Association of previous schistosome infection with diabetes and metabolic syndrome: a
826 cross-sectional study in rural China. *The Journal of clinical endocrinology and*
827 *metabolism* 98:E283-287.
828 Cnop, M., P.J. Havel, K.M. Utzschneider, D.B. Carr, M.K. Sinha, E.J. Boyko, B.M. Retzlaff, R.H.
829 Knopp, J.D. Brunzell, and S.E. Kahn. 2003. Relationship of adiponectin to body fat
830 distribution, insulin sensitivity and plasma lipoproteins: evidence for independent roles
831 of age and sex. *Diabetologia* 46:459-469.
832 Cortes-Selva, D., A.F. Elvington, A. Ready, B. Rajwa, E.J. Pearce, G.J. Randolph, and K.C. Fairfax.
833 2018a. Schistosoma mansoni Infection-Induced Transcriptional Changes in Hepatic
834 Macrophage Metabolism Correlate With an Athero-Protective Phenotype. *Frontiers in*
835 *Immunology* 9:
836 Cortes-Selva, D., A.F. Elvington, A. Ready, B. Rajwa, E.J. Pearce, G.J. Randolph, and K.C. Fairfax.
837 2018b. Schistosoma mansoni Infection-Induced Transcriptional Changes in Hepatic
838 Macrophage Metabolism Correlate With an Athero-Protective Phenotype. *Front*
839 *Immunol* 9:2580.
840 Cortes-Selva, D., L. Gibbs, J.A. Maschek, M. Nascimento, T. Van Ry, J.E. Cox, E. Amiel, and K.C.
841 Fairfax. 2021. Metabolic reprogramming of the myeloid lineage by Schistosoma mansoni
842 infection persists independently of antigen exposure. *PLoS pathogens* 17:e1009198.
843 Doenhoff, M.J., R.G. Stanley, K. Griffiths, and C.L. Jackson. 2002. An anti-atherogenic effect of
844 Schistosoma mansoni infections in mice associated with a parasite-induced lowering of
845 blood total cholesterol. *Parasitology* 125:415-421.
846 Edgar, R., M. Domrachev, and A.E. Lash. 2002. Gene Expression Omnibus: NCBI gene expression
847 and hybridization array data repository. *Nucleic Acids Res* 30:207-210.
848 Emerging Risk Factors, C., N. Sarwar, P. Gao, S.R. Seshasai, R. Gobin, S. Kaptoge, E. Di
849 Angelantonio, E. Ingelsson, D.A. Lawlor, E. Selvin, M. Stampfer, C.D. Stehouwer, S.
850 Lewington, L. Pennells, A. Thompson, N. Sattar, I.R. White, K.K. Ray, and J. Danesh. 2010.
851 Diabetes mellitus, fasting blood glucose concentration, and risk of vascular disease: a
852 collaborative meta-analysis of 102 prospective studies. *Lancet* 375:2215-2222.
853 Ewels, P., M. Magnusson, S. Lundin, and M. Kaller. 2016. MultiQC: summarize analysis results
854 for multiple tools and samples in a single report. *Bioinformatics* 32:3047-3048.
855 Fairfax, K.C., B. Everts, A.M. Smith, and E.J. Pearce. 2013. Regulation of the development of the
856 hepatic B cell compartment during Schistosoma mansoni infection. *J Immunol* 191:4202-
857 4210.
858 Friday, K.E., C. Dong, and R.U. Fontenot. 2001. Conjugated equine estrogen improves glycemic
859 control and blood lipoproteins in postmenopausal women with type 2 diabetes. *The*
860 *Journal of clinical endocrinology and metabolism* 86:48-52.
861 Griffin, C., N. Lanzetta, L. Eter, and K. Singer. 2016. Sexually dimorphic myeloid inflammatory
862 and metabolic responses to diet-induced obesity. *American journal of physiology.*
863 *Regulatory, integrative and comparative physiology* 311:R211-216.

Heianza, Y., Y. Arase, S. Kodama, S.D. Hsieh, H. Tsuji, K. Saito, H. Shimano, S. Hara, and H. Sone. 2013. Effect of postmenopausal status and age at menopause on type 2 diabetes and prediabetes in Japanese individuals: Toranomon Hospital Health Management Center Study 17 (TOPICS 17). *Diabetes Care* 36:4007-4014.

Herbert, D.R., C. Holscher, M. Mohrs, B. Arendse, A. Schwegmann, M. Radwanska, M. Leeto, R. Kirsch, P. Hall, H. Mossmann, B. Claussen, I. Forster, and F. Brombacher. 2004. Alternative macrophage activation is essential for survival during schistosomiasis and downmodulates T helper 1 responses and immunopathology. *Immunity* 20:623-635.

Hervouet, E., P. Peixoto, R. Delage-Mourroux, M. Boyer-Guittaut, and P.F. Cartron. 2018. Specific or not specific recruitment of DNMTs for DNA methylation, an epigenetic dilemma. *Clinical epigenetics* 10:17.

Hinton, W., A. McGovern, R. Coyle, T.S. Han, P. Sharma, A. Correa, F. Ferreira, and S. de Lusignan. 2018. Incidence and prevalence of cardiovascular disease in English primary care: a cross-sectional and follow-up study of the Royal College of General Practitioners (RCGP) Research and Surveillance Centre (RSC). *BMJ Open* 8:e020282.

Huang, S.C., B. Everts, Y. Ivanova, D. O'Sullivan, M. Nascimento, A.M. Smith, W. Beatty, L. Love-Gregory, W.Y. Lam, C.M. O'Neill, C. Yan, H. Du, N.A. Abumrad, J.F. Urban, Jr., M.N. Artyomov, E.L. Pearce, and E.J. Pearce. 2014. Cell-intrinsic lysosomal lipolysis is essential for alternative activation of macrophages. *Nature immunology* 15:846-855.

Huck, I., E.M. Morris, J. Thyfault, and U. Apte. 2021. Hepatocyte-Specific Hepatocyte Nuclear Factor 4 Alpha (HNF4) Deletion Decreases Resting Energy Expenditure by Disrupting Lipid and Carbohydrate Homeostasis. *Gene Expr* 20:157-168.

Humphries, K.H., M. Izadnegahdar, T. Sedlak, J. Saw, N. Johnston, K. Schenck-Gustafsson, R.U. Shah, V. Regitz-Zagrosek, J. Grewal, V. Vaccarino, J. Wei, and C.N. Bairey Merz. 2017. Sex differences in cardiovascular disease - Impact on care and outcomes. *Front Neuroendocrinol* 46:46-70.

Huo, Y., X. Guo, H. Li, H. Xu, V. Halim, W. Zhang, H. Wang, Y.Y. Fan, K.T. Ong, S.L. Woo, R.S. Chapkin, D.G. Mashek, Y. Chen, H. Dong, F. Lu, L. Wei, and C. Wu. 2012. Targeted overexpression of inducible 6-phosphofructo-2-kinase in adipose tissue increases fat deposition but protects against diet-induced insulin resistance and inflammatory responses. *The Journal of biological chemistry* 287:21492-21500.

Kim, S.H., and G. Reaven. 2013. Sex differences in insulin resistance and cardiovascular disease risk. *J Clin Endocrinol Metab* 98:E1716-1721.

Koelmel, J.P., N.M. Kroeger, C.Z. Ulmer, J.A. Bowden, R.E. Patterson, J.A. Cochran, C.W.W. Beecher, T.J. Garrett, and R.A. Yost. 2017. LipidMatch: an automated workflow for rule-based lipid identification using untargeted high-resolution tandem mass spectrometry data. *BMC Bioinformatics* 18:331.

Koh, J.H., M.L. Johnson, S. Dasari, N.K. LeBrasseur, I. Vuckovic, G.C. Henderson, S.A. Cooper, S. Manjunatha, G.N. Ruegsegger, G.I. Shulman, I.R. Lanza, and K.S. Nair. 2019. TFAM Enhances Fat Oxidation and Attenuates High-Fat Diet-Induced Insulin Resistance in Skeletal Muscle. *Diabetes* 68:1552-1564.

Koh, J.H., Y.W. Kim, D.Y. Seo, and T.S. Sohn. 2021. Mitochondrial TFAM as a Signaling Regulator between Cellular Organelles: A Perspective on Metabolic Diseases. *Diabetes Metab J* 45:853-865.

908 Kurylowicz, A., M. Jonas, W. Lisik, M. Jonas, Z.A. Wicik, Z. Wierzbicki, A. Chmura, and M.
909 Puzianowska-Kuznicka. 2015. Obesity is associated with a decrease in expression but not
910 with the hypermethylation of thermogenesis-related genes in adipose tissues. *J Transl*
911 *Med* 13:31.
912 Lapid, K., A. Lim, D.J. Clegg, D. Zeve, and J.M. Graff. 2014. Oestrogen signalling in white adipose
913 progenitor cells inhibits differentiation into brown adipose and smooth muscle cells. *Nat*
914 *Commun* 5:5196.
915 Laughlin-Tommaso, S.K., Z. Khan, A.L. Weaver, C.Y. Smith, W.A. Rocca, and E.A. Stewart. 2018.
916 Cardiovascular and metabolic morbidity after hysterectomy with ovarian conservation: a
917 cohort study. *Menopause* 25:483-492.
918 Lee, S.R., W.Y. Choi, J.H. Heo, J. Huh, G. Kim, K.P. Lee, H.J. Kwun, H.J. Shin, I.J. Baek, and E.J.
919 Hong. 2020. Progesterone increases blood glucose via hepatic progesterone receptor
920 membrane component 1 under limited or impaired action of insulin. *Sci Rep* 10:16316.
921 Lee, S.R., S.W. Kwon, P. Kaya, Y.H. Lee, J.G. Lee, G. Kim, G.S. Lee, I.J. Baek, and E.J. Hong. 2018.
922 Loss of progesterone receptor membrane component 1 promotes hepatic steatosis via
923 the induced de novo lipogenesis. *Sci Rep* 8:15711.
924 Li, H., D. Konja, L. Wang, and Y. Wang. 2022. Sex Differences in Adiposity and Cardiovascular
925 Diseases. *Int J Mol Sci* 23:
926 Marks, J.B., and P. Raskin. 2000. Cardiovascular risk in diabetes: a brief review. *J Diabetes*
927 *Complications* 14:108-115.
928 Matyash, V., G. Liebisch, T.V. Kurzchalia, A. Shevchenko, and D. Schwudke. 2008. Lipid
929 extraction by methyl-tert-butyl ether for high-throughput lipidomics. *J Lipid Res*
930 49:1137-1146.
931 Mejhert, N., L. Kuruvilla, K.R. Gabriel, S.D. Elliott, M.A. Guie, H. Wang, Z.W. Lai, E.A. Lane, R.
932 Christiano, N.N. Danial, R.V. Farese, Jr., and T.C. Walther. 2020. Partitioning of MLX-
933 Family Transcription Factors to Lipid Droplets Regulates Metabolic Gene Expression.
934 *Molecular cell* 77:1251-1264 e1259.
935 Moran, A., D.R. Jacobs, Jr., J. Steinberger, L.M. Steffen, J.S. Pankow, C.P. Hong, and A.R. Sinaiko.
936 2008. Changes in insulin resistance and cardiovascular risk during adolescence:
937 establishment of differential risk in males and females. *Circulation* 117:2361-2368.
938 Ng, M.K., W. Jessup, and D.S. Celermajer. 2001. Sex-related differences in the regulation of
939 macrophage cholesterol metabolism. *Curr Opin Lipidol* 12:505-510.
940 Opotowsky, A.R., J.M. McWilliams, and C.P. Cannon. 2007. Gender differences in aspirin use
941 among adults with coronary heart disease in the United States. *J Gen Intern Med* 22:55-
942 61.
943 Peters, S.A., R.R. Huxley, and M. Woodward. 2014. Diabetes as risk factor for incident coronary
944 heart disease in women compared with men: a systematic review and meta-analysis of
945 64 cohorts including 858,507 individuals and 28,203 coronary events. *Diabetologia*
946 57:1542-1551.
947 Picard, F., M. Wanatabe, K. Schoonjans, J. Lydon, B.W. O'Malley, and J. Auwerx. 2002.
948 Progesterone receptor knockout mice have an improved glucose homeostasis secondary
949 to beta -cell proliferation. *Proceedings of the National Academy of Sciences of the*
950 *United States of America* 99:15644-15648.

Qi, T., Y. Chen, H. Li, Y. Pei, S.L. Woo, X. Guo, J. Zhao, X. Qian, J. Awika, Y. Huo, and C. Wu. 2017. A role for PFKFB3/iPFK2 in metformin suppression of adipocyte inflammatory responses. *J Mol Endocrinol* 59:49-59.

Robinson, M.D., D.J. McCarthy, and G.K. Smyth. 2010. edgeR: a Bioconductor package for differential expression analysis of digital gene expression data. *Bioinformatics* 26:139-140.

Roth, G.A., C. Johnson, A. Abajobir, F. Abd-Allah, S.F. Abera, G. Abyu, M. Ahmed, B. Aksut, T. Alam, K. Alam, F. Alla, N. Alvis-Guzman, S. Amrock, H. Ansari, J. Arnlov, H. Asayesh, T.M. Atey, L. Avila-Burgos, A. Awasthi, A. Banerjee, A. Barac, T. Barnighausen, L. Barregard, N. Bedi, E. Belay Ketema, D. Bennett, G. Berhe, Z. Bhutta, S. Bitew, J. Carapetis, J.J. Carrero, D.C. Malta, C.A. Castaneda-Orjuela, J. Castillo-Rivas, F. Catala-Lopez, J.Y. Choi, H. Christensen, M. Cirillo, L. Cooper, Jr., M. Criqui, D. Cundiff, A. Damasceno, L. Dandona, R. Dandona, K. Davletov, S. Dharmaratne, P. Dorairaj, M. Dubey, R. Ehrenkranz, M. El Sayed Zaki, E.J.A. Faraon, A. Esteghamati, T. Farid, M. Farvid, V. Feigin, E.L. Ding, G. Fowkes, T. Gebrehiwot, R. Gillum, A. Gold, P. Gona, R. Gupta, T.D. Habtewold, N. Hafezi-Nejad, T. Hailu, G.B. Hailu, G. Hankey, H.Y. Hassen, K.H. Abate, R. Havmoeller, S.I. Hay, M. Horino, P.J. Hotez, K. Jacobsen, S. James, M. Javanbakht, P. Jeemon, D. John, J. Jonas, Y. Kalkonde, C. Karimkhani, A. Kasaeian, Y. Khader, A. Khan, Y.H. Khang, S. Khera, A.T. Khoja, J. Khubchandani, D. Kim, D. Kolte, S. Kosen, K.J. Krohn, G.A. Kumar, G.F. Kwan, D.K. Lal, A. Larsson, S. Linn, A. Lopez, P.A. Lotufo, H.M.A. El Razek, R. Malekzadeh, M. Mazidi, T. Meier, K.G. Meles, G. Mensah, A. Meretoja, H. Mezgebe, T. Miller, E. Mirrakhimov, S. Mohammed, A.E. Moran, K.I. Musa, J. Narula, B. Neal, F. Ngalesoni, G. Nguyen, C.M. Obermeyer, M. Owolabi, G. Patton, J. Pedro, D. Qato, M. Qorbani, K. Rahimi, R.K. Rai, S. Rawaf, A. Ribeiro, S. Safiri, J.A. Salomon, I. Santos, M. Santric Milicevic, B. Sartorius, A. Schutte, S. Sepanlou, M.A. Shaikh, M.J. Shin, M. Shishehbor, H. Shore, D.A.S. Silva, E. Sobngwi, S. Stranges, S. Swaminathan, R. Tabares-Seisdedos, N. Tadele Atnafu, F. Tesfay, J.S. Thakur, A. Thrift, R. Topor-Madry, T. Truelsen, S. Tyrovolas, K.N. Ukwaja, O. Uthman, T. Vasankari, V. Vlassov, S.E. Vollset, T. Wakayo, D. Watkins, R. Weintraub, A. Werdecker, R. Westerman, C.S. Wiysonge, C. Wolfe, A. Workicho, G. Xu, Y. Yano, P. Yip, N. Yonemoto, M. Younis, C. Yu, T. Vos, M. Naghavi, and C. Murray. 2017. Global, Regional, and National Burden of Cardiovascular Diseases for 10 Causes, 1990 to 2015. *J Am Coll Cardiol* 70:1-25.

Rubinow, K.B. 2018. An intracrine view of sex steroids, immunity, and metabolic regulation. *Mol Metab* 15:92-103.

Rudyk, M.P., V.V. Pozur, D.O. Voieikova, Y.V. Hurmach, N.M. Khranovska, O.V. Skachkova, V.M. Svyatetska, O.G. Fedorchuk, L.M. Skivka, T.V. Berehova, and L.I. Ostapchenko. 2018. Sex-based differences in phagocyte metabolic profile in rats with monosodium glutamate-induced obesity. *Sci Rep* 8:5419.

Sanya, R.E., E.L. Webb, C. Zziwa, R. Kizindo, M. Sewankambo, J. Tumusiime, E. Nakazibwe, G. Oduru, E. Niwagaba, P. Kabuubi Nakawungu, J. Kabagenyi, J. Nassuuna, B. Walusimbi, I.A. Biraro, A.M. Elliott, and V.t.t. La. 2019. The effect of helminth infections and their treatment on metabolic outcomes: results of a cluster-randomised trial. *Clinical infectious diseases : an official publication of the Infectious Diseases Society of America*

Satoh, J., N. Kawana, and Y. Yamamoto. 2013. Pathway Analysis of ChIP-Seq-Based NRF1 Target Genes Suggests a Logical Hypothesis of their Involvement in the Pathogenesis of Neurodegenerative Diseases. *Gene Regul Syst Bio* 7:139-152.

Shen, S.W., Y. Lu, F. Li, Z.H. Shen, M. Xu, W.F. Yao, Y.B. Feng, J.T. Yun, Y.P. Wang, W. Ling, H.J. Qi, and D.X. Tong. 2015. The potential long-term effect of previous schistosome infection reduces the risk of metabolic syndrome among Chinese men. *Parasite immunology* 37:333-339.

Singer, K., J. DelProposto, D.L. Morris, B. Zamarron, T. Mergian, N. Maley, K.W. Cho, L. Geletka, P. Subbaiah, L. Muir, G. Martinez-Santibanez, and C.N. Lumeng. 2014. Diet-induced obesity promotes myelopoiesis in hematopoietic stem cells. *Mol Metab* 3:664-675.

Stachowiak, G., T. Pertynski, and M. Pertynska-Marczewska. 2015. Metabolic disorders in menopause. *Prz Menopauzalny* 14:59-64.

Stanley, R.G., C.L. Jackson, K. Griffiths, and M.J. Doenhoff. 2009. Effects of Schistosoma mansoni worms and eggs on circulating cholesterol and liver lipids in mice. *Atherosclerosis* 207:131-138.

Svendsen, O.L., C. Hassager, and C. Christiansen. 1995. Age- and menopause-associated variations in body composition and fat distribution in healthy women as measured by dual-energy X-ray absorptiometry. *Metabolism* 44:369-373.

Tan, Y.Y., G.C. Gast, and Y.T. van der Schouw. 2010. Gender differences in risk factors for coronary heart disease. *Maturitas* 65:149-160.

Taneja, V. 2018. Sex Hormones Determine Immune Response. *Front Immunol* 9:1931.

Varghese, M., C. Griffin, S. Abrishami, L. Eter, N. Lanzetta, L. Hak, J. Clemente, D. Agarwal, A. Lerner, M. Westerhoff, R. Patel, E. Bowers, M. Islam, P. Subbaiah, and K. Singer. 2021. Sex hormones regulate metainflammation in diet-induced obesity in mice. *The Journal of biological chemistry* 297:101229.

Vats, D., L. Mukundan, J.I. Odegaard, L. Zhang, K.L. Smith, C.R. Morel, R.A. Wagner, D.R. Greaves, P.J. Murray, and A. Chawla. 2006. Oxidative metabolism and PGC-1beta attenuate macrophage-mediated inflammation. *Cell Metab* 4:13-24.

Vernia, S., J. Cavanagh-Kyros, T. Barrett, D.Y. Jung, J.K. Kim, and R.J. Davis. 2013. Diet-induced obesity mediated by the JNK/DIO2 signal transduction pathway. *Genes Dev* 27:2345-2355.

Wang, H., K. Divaris, B. Pan, X. Li, J.H. Lim, G. Saha, M. Barovic, D. Giannakou, J.M. Korostoff, Y. Bing, S. Sen, K. Moss, D. Wu, J.D. Beck, C.M. Ballantyne, P. Natarajan, K.E. North, M.G. Netea, T. Chavakis, and G. Hajishengallis. 2024. Clonal hematopoiesis driven by mutated DNMT3A promotes inflammatory bone loss. *Cell* 187:3690-3711 e3619.

Willeit, J., S. Kiechl, G. Egger, M. Oberhollenzer, F. Oberhollenzer, M. Muggeo, W. Poewe, and E. Bonora. 1997. The role of insulin in age-related sex differences of cardiovascular risk profile and morbidity. *Atherosclerosis* 130:183-189.

Wilson, J.E. 2003. Isozymes of mammalian hexokinase: structure, subcellular localization and metabolic function. *J Exp Biol* 206:2049-2057.

Winn, N.C., T.J. Jurrissen, Z.I. Grunewald, R.P. Cunningham, M.L. Woodford, J.A. Kanaley, D.B. Lubahn, C. Manrique-Acevedo, R.S. Rector, V.J. Vieira-Potter, and J. Padilla. 2019. Estrogen receptor-alpha signaling maintains immunometabolic function in males and is

obligatory for exercise-induced amelioration of nonalcoholic fatty liver. *Am J Physiol Endocrinol Metab* 316:E156-E167.

Wiria, A.E., F. Hamid, L.J. Wammes, M.A. Prasetyani, O.M. Dekkers, L. May, M.M. Kaisar, J.J. Verweij, B. Guigas, F. Partono, E. Sartono, T. Supali, M. Yazdanbakhsh, and J.W. Smit. 2015. Infection with Soil-Transmitted Helminths Is Associated with Increased Insulin Sensitivity. *PloS one* 10:e0127746.

Wolde, M., N. Berhe, G. Medhin, F. Chala, I. van Die, and A. Tsegaye. 2019. Inverse Associations of Schistosoma mansoni Infection and Metabolic Syndromes in Humans: A Cross-Sectional Study in Northeast Ethiopia. *Microbiol Insights* 12:1178636119849934.

Wolfs, I.M., J.L. Stoger, P. Goossens, C. Pottgens, M.J. Gijbels, E. Wijnands, E.P. van der Vorst, P. van Gorp, L. Beckers, D. Engel, E.A. Biessen, G. Kraal, I. van Die, M.M. Donners, and M.P. de Winther. 2014. Reprogramming macrophages to an anti-inflammatory phenotype by helminth antigens reduces murine atherosclerosis. *FASEB J* 28:288-299.

Wong, N.D., Y. Zhao, R. Patel, C. Patao, S. Malik, A.G. Bertoni, A. Correa, A.R. Folsom, S. Kachroo, J. Mukherjee, H. Taylor, and E. Selvin. 2016. Cardiovascular Risk Factor Targets and Cardiovascular Disease Event Risk in Diabetes: A Pooling Project of the Atherosclerosis Risk in Communities Study, Multi-Ethnic Study of Atherosclerosis, and Jackson Heart Study. *Diabetes Care* 39:668-676.

Wyatt, E., R. Wu, W. Rabeh, H.W. Park, M. Ghanefar, and H. Ardehali. 2010. Regulation and cytoprotective role of hexokinase III. *PloS one* 5:e13823.

Yan, H., W. Yang, F. Zhou, X. Li, Q. Pan, Z. Shen, G. Han, A. Newell-Fugate, Y. Tian, R. Majeti, W. Liu, Y. Xu, C. Wu, K. Allred, C. Allred, Y. Sun, and S. Guo. 2019. Estrogen Improves Insulin Sensitivity and Suppresses Gluconeogenesis via the Transcription Factor Foxo1. *Diabetes* 68:291-304.

Yoshida, Y., Z. Chen, V.A. Fonseca, and F. Mauvais-Jarvis. 2023. Sex Differences in Cardiovascular Risk Associated With Prediabetes and Undiagnosed Diabetes. *American journal of preventive medicine* 65:854-862.

Zhang, Y., B.V. Howard, L.D. Cowan, J. Yeh, C.F. Schaefer, R.A. Wild, W. Wang, and E.T. Lee. 2002. The effect of estrogen use on levels of glucose and insulin and the risk of type 2 diabetes in american Indian postmenopausal women : the strong heart study. *Diabetes Care* 25:500-504.

Zhao, T., J. Zhang, H. Lei, Y. Meng, H. Cheng, Y. Zhao, G. Geng, C. Mu, L. Chen, Q. Liu, Q. Luo, C. Zhang, Y. Long, J. Su, Y. Wang, Z. Li, J. Sun, G. Chen, Y. Li, X. Liao, Y. Shang, G. Hu, Q. Chen, and Y. Zhu. 2023. NRF1-mediated mitochondrial biogenesis antagonizes innate antiviral immunity. *The EMBO journal* 42:e113258.

A

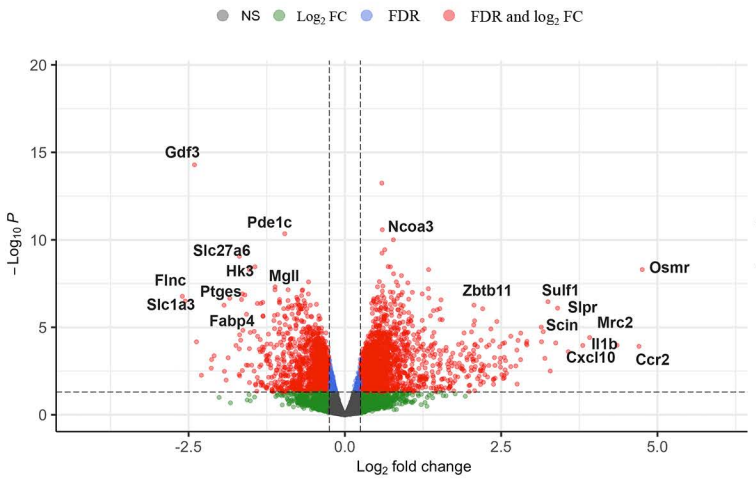
Uninfected Male Vs Uninfected Female
NS
Log2 FC
FDR
FDR and log2 FC
−Log10 P
Log2 fold change
Gdf3
Pde1c
Ncoa3
Slc27a6
Hk3
Mgll
Flnc
Ptges
Slc1a3
Fabp4
Zbtb11
Sulf1
Slpr
Scin
Mrc2
Il1b
Cxcl10
Ccr2
Osmr

B

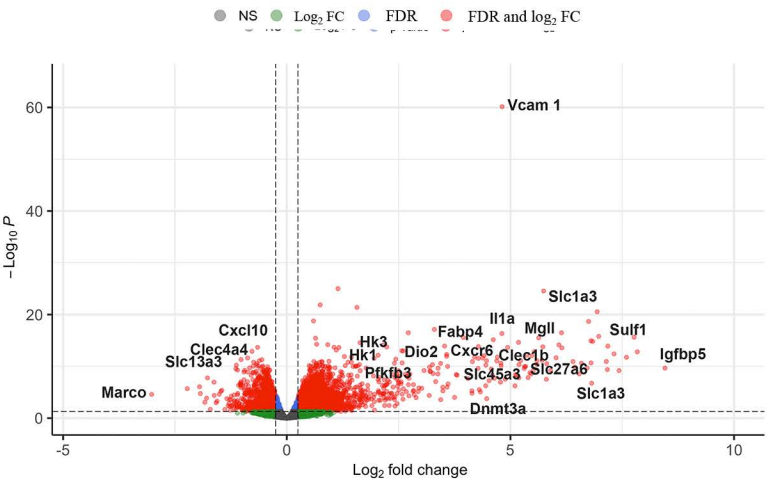
Infected Male Vs Infected Female
NS
Log2 FC
FDR
FDR and log2 FC
−Log10 P
Log2 fold change
Vcam 1
Slc1a3
Il1a
Mgll
Sulf1
Cxcl10
Clec4a4
Slc13a3
Hk3
Hk1
Fabp4
Dio2
Cxcr6
Clec1b
Slc27a6
Igfbp5
Pfkfb3
Slc45a3
Marco
Dnmt3a
Slc1a3

C

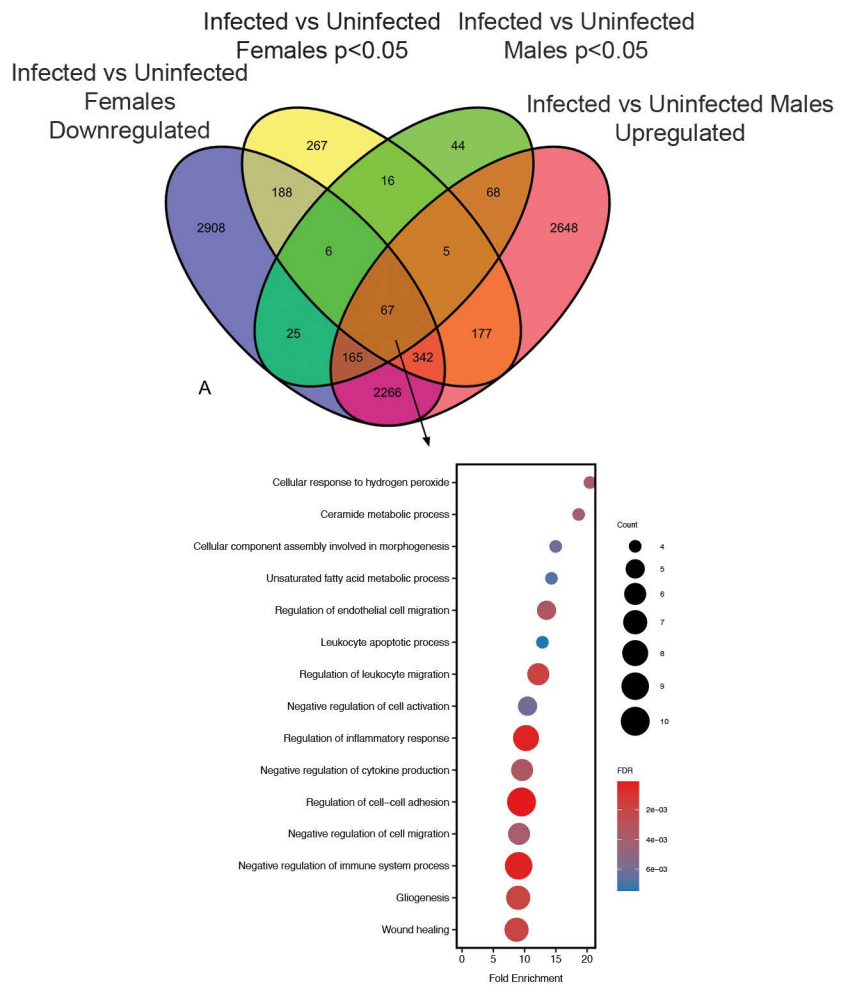
Differential transcriptional regulation by infection in Males vs Females
Infected vs Uninfected Females p<0.05
Infected vs Uninfected Males p<0.05
Infected vs Uninfected Females Downregulated
Infected vs Uninfected Males Upregulated
267
44
188
16
68
2908
6
5
2648
67
25
177
165
342
2266
A
Cellular response to hydrogen peroxide
Ceramide metabolic process
Cellular component assembly involved in morphogenesis
Unsaturated fatty acid metabolic process
Regulation of endothelial cell migration
Leukocyte apoptotic process
Regulation of leukocyte migration
Negative regulation of cell activation
Regulation of inflammatory response
Negative regulation of cytokine production
Regulation of cell−cell adhesion
Negative regulation of cell migration
Negative regulation of immune system process
Gliogenesis
Wound healing
Count
FDR
Fold Enrichment

D

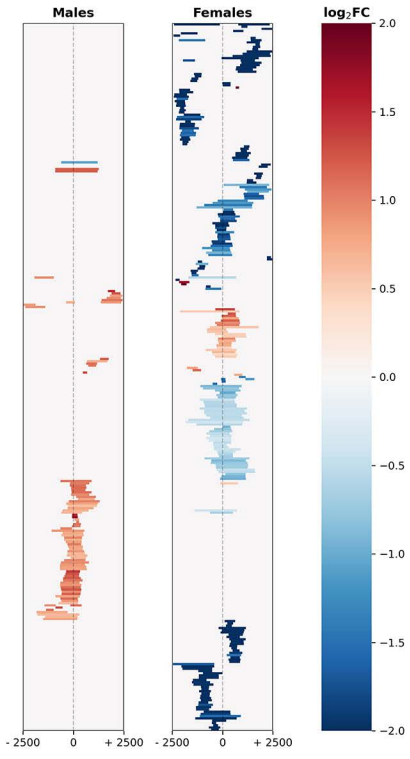
ATAC-seq Differentially accessible peaks around TSS
Males
Females
log2FC
- 2500
0
+ 2500

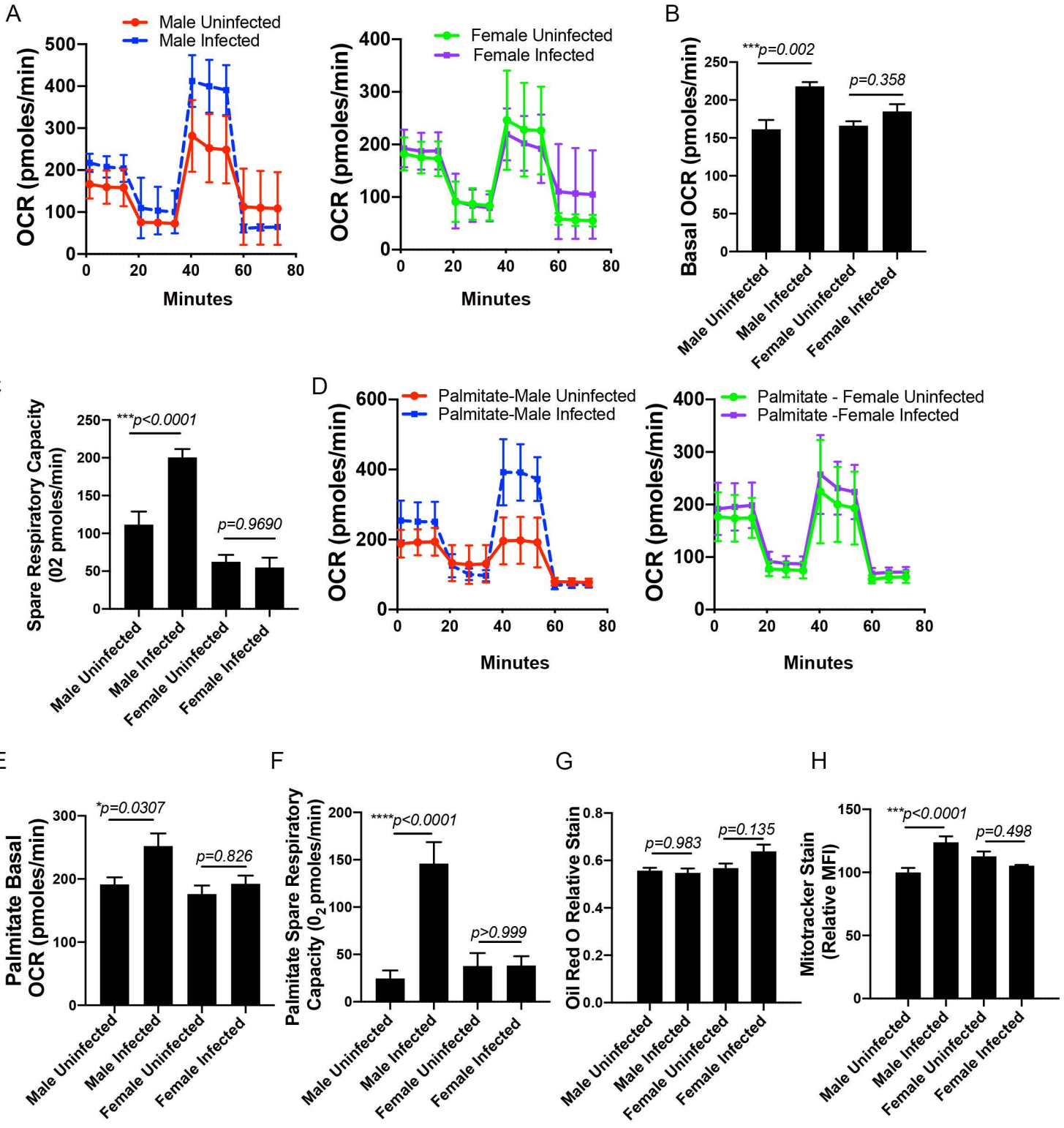
A
Male Uninfected
Male Infected
OCR (pmoles/min)
Minutes
Female Uninfected
Female Infected
B
***p=0.002
p=0.358
Basal OCR (pmoles/min)
Male Uninfected
Male Infected
Female Uninfected
Female Infected
C
***p<0.0001
p=0.9690
Spare Respiratory Capacity (02 pmoles/min)
D
Palmitate-Male Uninfected
Palmitate-Male Infected
Palmitate - Female Uninfected
Palmitate -Female Infected
E
*p=0.0307
p=0.826
Palmitate Basal OCR (pmoles/min)
F
****p<0.0001
p>0.999
Palmitate Spare Respiratory Capacity (02 pmoles/min)
G
p=0.983
p=0.135
Oil Red O Relative Stain
H
***p<0.0001
p=0.498
Mitotracker Stain (Relative MFI)

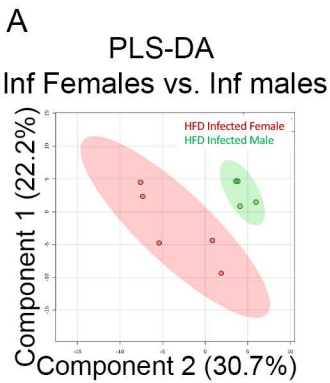
A
PLS-DA
Inf Females vs. Inf males
HFD Infected Female
HFD Infected Male
Component 1 (22.2%)
Component 2 (30.7%)

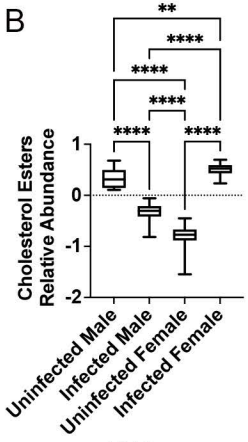
B
Cholesterol Esters
Relative Abundance
Uninfected Male
Infected Male
Uninfected Female
Infected Female

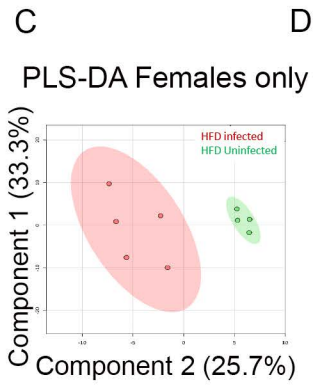
C
PLS-DA Females only
HFD infected
HFD Uninfected
Component 1 (33.3%)
Component 2 (25.7%)

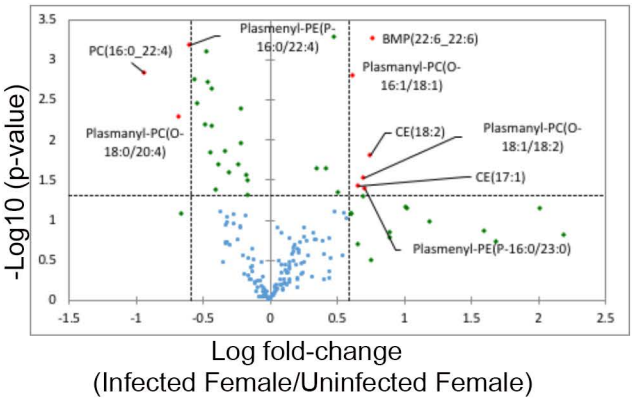
D
PC(16:0_22:4)
Plasmenyl-PE(P-16:0/22:4)
BMP(22:6_22:6)
Plasmanyl-PC(O-16:1/18:1)
Plasmanyl-PC(O-18:0/20:4)
CE(18:2)
Plasmanyl-PC(O-18:1/18:2)
CE(17:1)
Plasmenyl-PE(P-16:0/23:0)
-Log10 (p-value)
Log fold-change
(Infected Female/Uninfected Female)

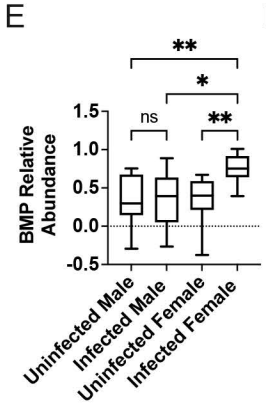
E
BMP Relative Abundance
Uninfected Male
Infected Male
Uninfected Female
Infected Female

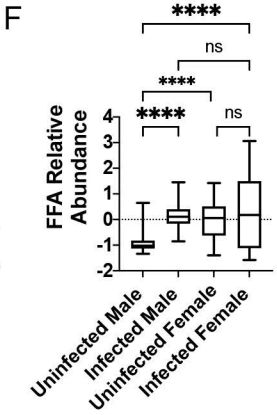
F
FFA Relative Abundance
Uninfected Male
Infected Male
Uninfected Female
Infected Female

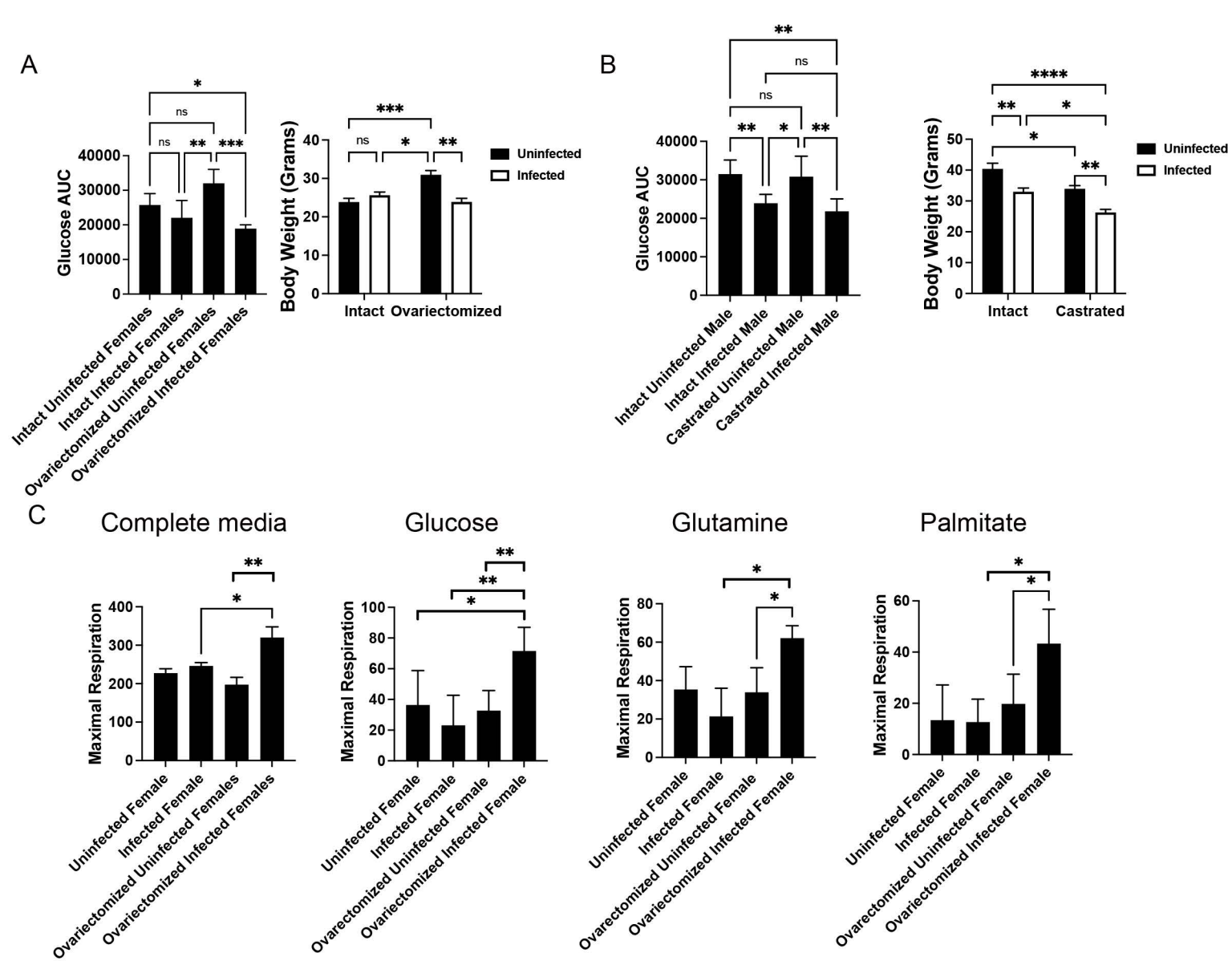
A
Glucose AUC
40000
30000
20000
10000
0
*
ns
ns
**
***
Intact Uninfected Females
Intact Infected Females
Ovariectomized Uninfected Females
Ovariectomized Infected Females
Body Weight (Grams)
40
30
20
10
0
***
ns
*
**
Intact
Ovariectomized
Uninfected
Infected
B
Glucose AUC
40000
30000
20000
10000
0
**
ns
ns
**
*
**
Intact Uninfected Male
Intact Infected Male
Castrated Uninfected Male
Castrated Infected Male
Body Weight (Grams)
50
40
30
20
10
0
****
**
*
*
**
Intact
Castrated
Uninfected
Infected
C
Complete media
Maximal Respiration
400
300
200
100
0
**
*
Uninfected Female
Infected Female
Ovarectomized Uninfected Females
Ovariectomized Infected Females
Glucose
Maximal Respiration
100
80
60
40
20
0
**
**
*
Uninfected Female
Infected Female
Ovarectomized Uninfected Female
Ovariectomized Infected Female
Glutamine
Maximal Respiration
80
60
40
20
0
*
*
Uninfected Female
Infected Female
Ovarectomized Uninfected Female
Ovariectomized Infected Female
Palmitate
Maximal Respiration
60
40
20
0
*
*
Uninfected Female
Infected Female
Ovarectomized Uninfected Female
Ovariectomized Infected Female

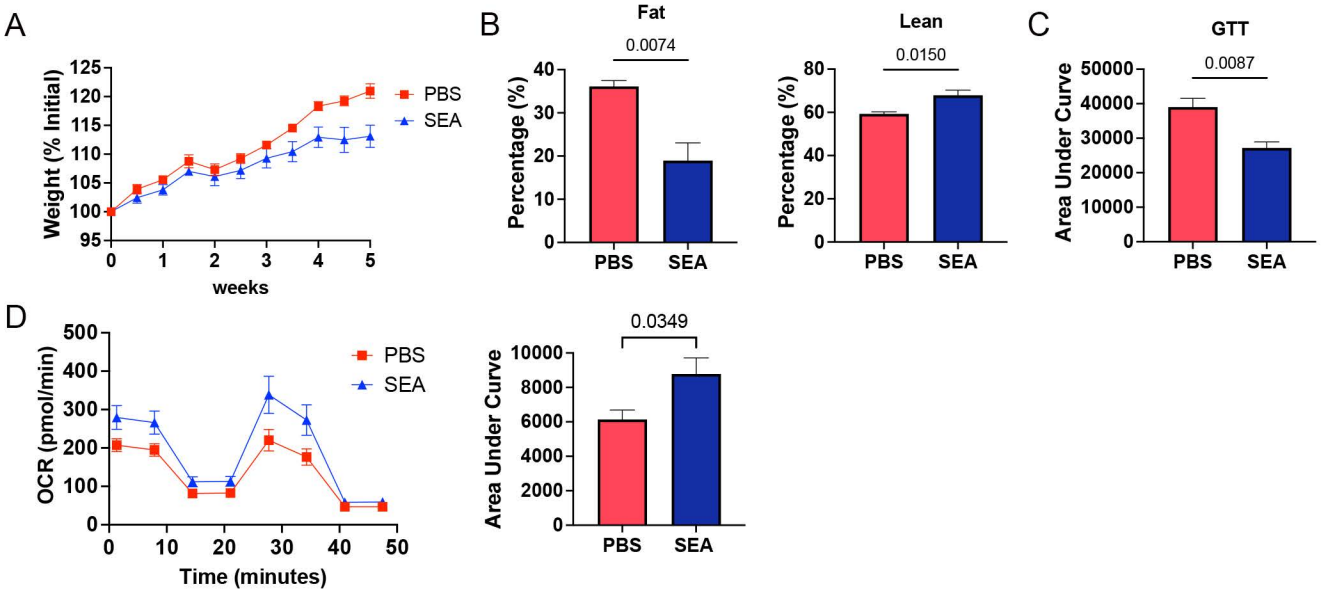
A
Weight (% Initial)
125
120
115
110
105
100
95
0
1
2
3
4
5
weeks
PBS
SEA
B
Fat
0.0074
Percentage (%)
40
30
20
10
0
PBS
SEA
Lean
0.0150
Percentage (%)
80
60
40
20
0
PBS
SEA
C
GTT
0.0087
Area Under Curve
50000
40000
30000
20000
10000
0
PBS
SEA
D
OCR (pmol/min)
500
400
300
200
100
0
0
10
20
30
40
50
Time (minutes)
PBS
SEA
0.0349
Area Under Curve
10000
8000
6000
4000
2000
0
PBS
SEA

Males

Females

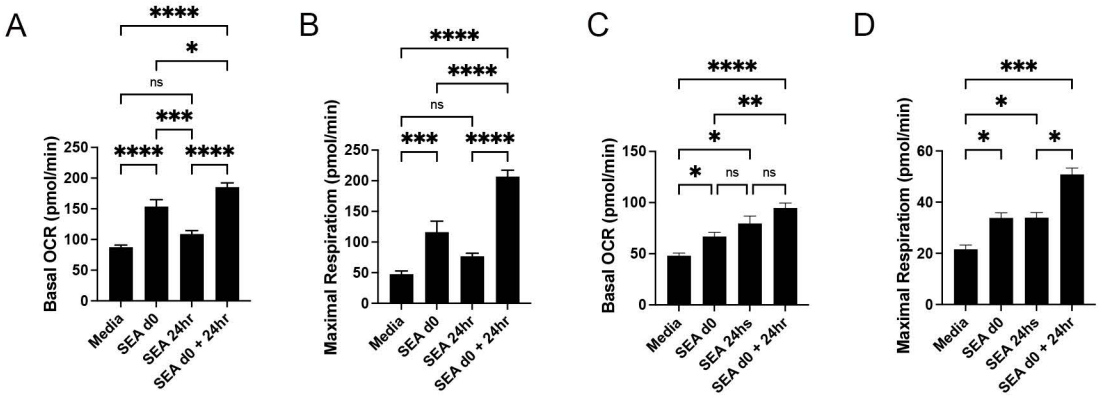

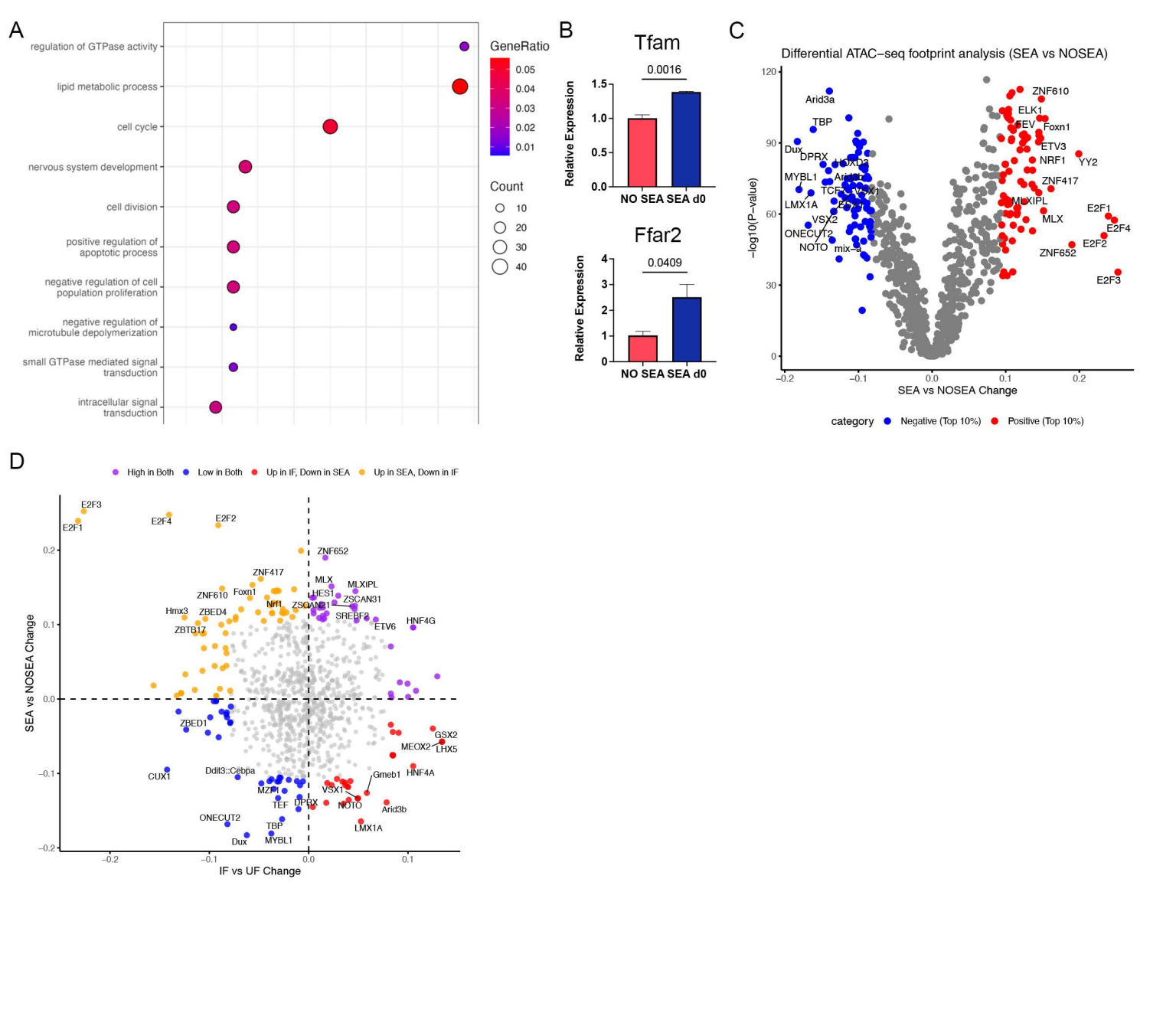
A
regulation of GTPase activity
lipid metabolic process
cell cycle
nervous system development
cell division
positive regulation of apoptotic process
negative regulation of cell population proliferation
negative regulation of microtubule depolymerization
small GTPase mediated signal transduction
intracellular signal transduction
GeneRatio
0.05
0.04
0.03
0.02
0.01
Count
10
20
30
40
B
Tfam
0.0016
Relative Expression
NO SEA SEA d0
Ffar2
0.0409
Relative Expression
NO SEA SEA d0
C
Differential ATAC−seq footprint analysis (SEA vs NOSEA)
−log10(P−value)
SEA vs NOSEA Change
category
Negative (Top 10%)
Positive (Top 10%)
ZNF610
ELK1
FEV
Foxn1
ETV3
NRF1
YY2
ZNF417
MLXIPL
MLX
E2F1
E2F4
E2F2
E2F3
ZNF652
Arid3a
TBP
Dux
DPRX
MYBL1
LMX1A
VSX2
ONECUT2
NOTO
mix−a
D
High in Both
Low in Both
Up in IF, Down in SEA
Up in SEA, Down in IF
SEA vs NOSEA Change
IF vs UF Change
E2F3
E2F1
E2F4
E2F2
ZNF652
ZNF417
MLX
MLXIPL
ZNF610
Foxn1
HES1
ZSCAN31
Nfi1
ZSCAN21
SREBF2
Hmx3
ZBED4
ZBTB17
ETV6
HNF4G
ZBED1
GSX2
MEOX2
LHX5
CUX1
Ddit3::Cebpa
Gmeb1
HNF4A
MZF1
VSX1
TEF
DPRX
NOTO
Arid3b
ONECUT2
TBP
LMX1A
Dux
MYBL1

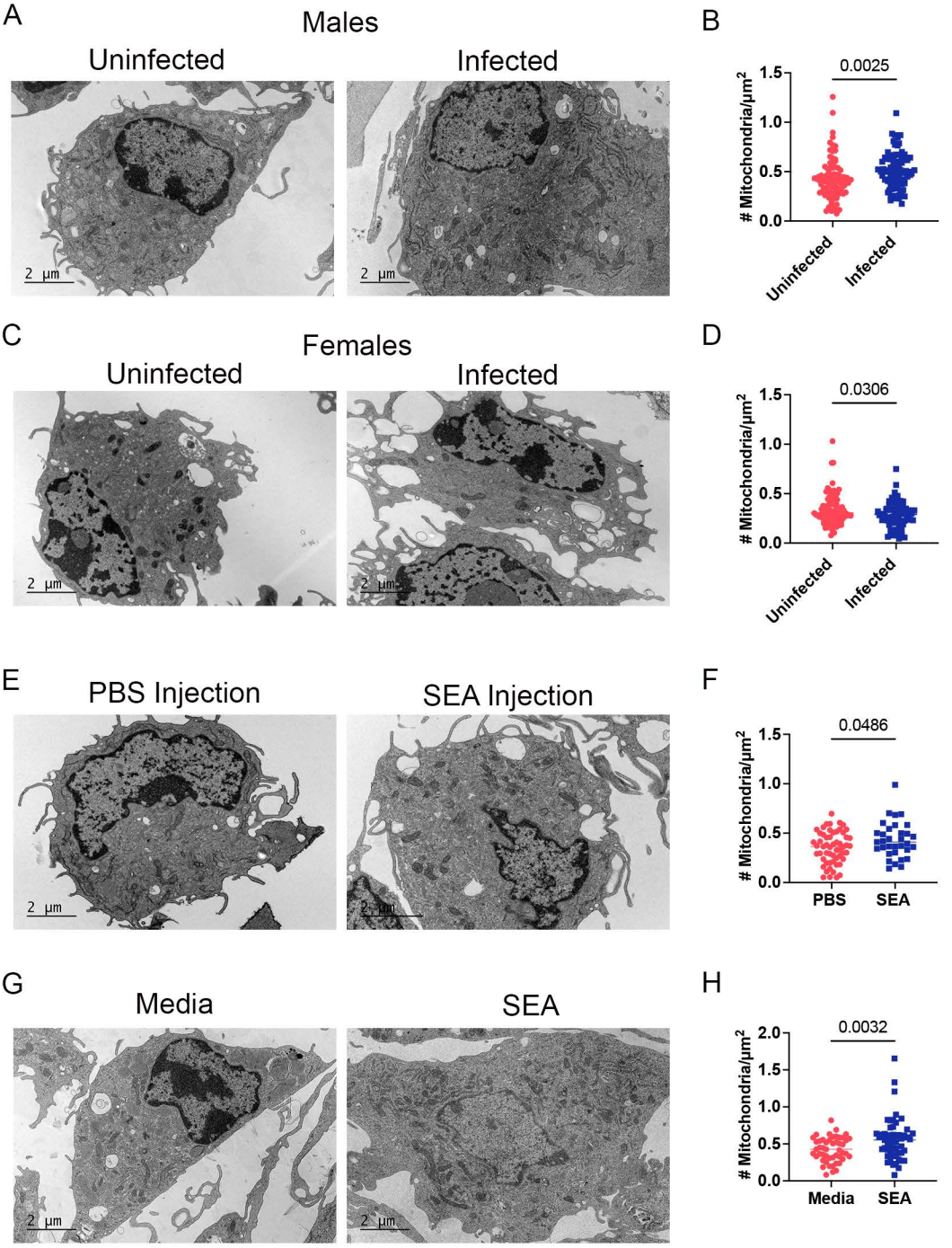
A
Males
Uninfected
Infected
2 µm
2 µm
B
0.0025
Mitochondria/µm²
1.5
1.0
0.5
0.0
Uninfected
Infected
C
Females
Uninfected
Infected
2 µm
2 µm
D
0.0306
Mitochondria/µm²
1.5
1.0
0.5
0.0
Uninfected
Infected
E
PBS Injection
SEA Injection
2 µm
2 µm
F
0.0486
Mitochondria/µm²
1.5
1.0
0.5
0.0
PBS
SEA
G
Media
SEA
2 µm
2 µm
H
0.0032
Mitochondria/µm²
2.0
1.5
1.0
0.5
0.0
Media
SEA